


Forecasting high-dimensional functional time series with dual-factor structures

Chen Tang  *

Research School of Finance, Actuarial Studies and Statistics
Australian National University

Han Lin Shang 

Department of Actuarial Studies and Business Analytics
Macquarie University

Yanrong Yang 

Research School of Finance, Actuarial Studies and Statistics
Australian National University

Yang Yang 

School of Information and Physical Sciences
The University of Newcastle

Abstract

We propose a dual-factor model for high-dimensional functional time series (HDFTS) that considers multiple populations. The HDFTS is first decomposed into a collection of functional time series (FTS) in a lower dimension and a group of population-specific basis functions. The system of basis functions describes cross-sectional heterogeneity, while the reduced-dimension FTS retains most of the information common to multiple populations. The low-dimensional FTS is further decomposed into a product of common functional loadings and a matrix-valued time series that contains the most temporal dynamics embedded in the original HDFTS. The proposed general-form dual-factor structure is connected to several commonly used functional factor models. We demonstrate the finite-sample performances of the proposed method in recovering cross-sectional basis functions and extracting common features using simulated HDFTS. An empirical study shows that the proposed model produces more accurate point and interval forecasts for subnational age-specific mortality rates in Japan. The financial benefits associated with the improved mortality forecasts are translated into a life annuity pricing scheme.

Keywords: Age-specific mortality forecasting; Factor models; Functional panel data; Functional principal component analysis; Multilevel functional data.

*Postal address: Research School of Finance, Actuarial Studies and Statistics, Level 4, Building 26C, Australian National University, Kingsley Street, Acton, Canberra, ACT 2601, Australia; Email: chen.tang@anu.edu.au.

1 Introduction

Increased human life expectancy brings longevity risks to governments, health care systems and life insurance industries. Government stakeholders and industry practitioners need accurate and easily understandable mortality forecasting methods to help them gauge the risks associated with extended longevity. Modelling and forecasting age-specific mortality rates have become an ongoing research endeavour, noting particularly the seminal work by [Lee and Carter \(1992\)](#) advancing the field of research. However, the Lee-Carter model and many of its extensions and modifications (see, e.g., [Renshaw and Haberman, 2003](#); [Li et al., 2013](#); [Wiśniowski et al., 2015](#)) consider only a single population. A common disadvantage of such univariate mortality modelling methods is that they tend to produce divergent forecasts for a group of related populations over relatively long forecast horizons. As a remedy, coherent mortality forecasting methods (see, e.g., [Pampel, 2005](#); [Li and Lee, 2005](#); [Li, 2013](#)) that simultaneously consider multiple populations have gained popularity in recent years. This is because jointly modelling multiple closely related mortality series facilitates the pooling of common information of the considered populations and hence results in improved forecasts ([Shang, 2016](#); [Jiménez-Varón et al., 2024](#)).

However, the aforementioned multivariate mortality modelling methods cannot handle high-dimensional multi-population mortality data. When working with mortality data in which the number of populations (cross-sectional units) is comparable to, or even more significant than, the observation years (sample size of FTS), many conventional statistical tools tend to fail, and high-dimensional data analysis techniques are needed (see, e.g., [Cai and Chen, 2010](#); [Bühlmann and van de Geer, 2011](#)). In addition, various populations (e.g., different countries) may report mortality rates over different time intervals. Limiting the mortality observations to the same time is often necessary before applying the conventional matrix-based multivariate mortality models (e.g., the extended Lee-Carter model of [Li et al., 2013](#)).

To solve these problems, we propose to model multi-population mortality time series in a functional data analysis framework with high-dimensional data analysis techniques. In this functional data analysis setting, the age-specific mortality rates at any given year can be regarded as a curve; hence the curves relate to any particular population and are recorded sequentially according to time form FTS (see, e.g., [Ramsay and Silverman, 2006](#); [Hörmann and Kokoszka, 2010](#)). In the analysis of FTS, dimension-reduction techniques, such as functional principal component analysis (FPCA), are necessary to collapse the infinite-dimensional curves into a series of orthonormal basis

functions and their corresponding matrix-valued coefficients. To handle the high dimensionality of data related to a large number of populations, factor analysis is often used to reduce the variation contained in multi-population data into a smaller number of uncorrelated factors (see, e.g., [Bai and Ng, 2008](#)). When applying our proposed method to multi-population mortality data, we employ both dimension-reduction techniques to solve the two-fold “curse of dimensionality” ([Bellman, 1966](#)).

The key contributions of this study are as follows.

- 1) We propose a dual-factor structure for modelling and forecasting high-dimensional functional time series (HDFTS). The proposed method effectively decomposes HDFTS into the product of a vector of common loading (front-loading) functions, a low-dimensional matrix-valued time series, and a finite collection of factor loading (back-loading) functions. When applied to the analysis of high-dimensional mortality data, our method retains common age characteristics of human mortality curves in the front-loadings and identifies region-specific features over age in the back factor loadings. In addition, temporal dynamics of the original HDFTS are captured by the low-dimensional matrix-valued time series that facilitates forecasting.
- 2) The proposed general-form dual-factor structure covers several commonly used functional factor models as special cases. By selecting the appropriate front and back-loading functions, the proposed general dual-factor model structure can be extended to several existing models in the literature.
- 3) Using a Monte Carlo simulation study, we demonstrate the finite-sample performance of the proposed method in recovering cross-sectional heterogeneous basis functions and extracting common features.
- 4) In an empirical analysis of Japanese subnational mortality rates, we further demonstrate the HDFTS model’s ability to produce more accurate point and interval forecasts than several commonly used multi-population mortality models. Moreover, we demonstrate the financial impact of the accurate forecasts produced by our model on life annuity pricing. It is shown that the proposed model could result in significant savings for the insurance providers’ reserve funds.

2 Related work

Early attempts at jointly modelling multivariate FTS in the literature, include, for example, the work of [Di et al. \(2009\)](#), which introduced the multilevel FPCA that performs the conventional FPCA on intra- and inter-subject geometric components of multilevel functional data. [Shang \(2016\)](#) applied multilevel FPCA to model the mortality rates of multiple populations. To consider functional data exhibiting significant heterogeneity, [Tang et al. \(2022\)](#) proposed a clustering method capable of grouping multiple FTS into homogeneous sets before jointly modelling the curves in each set. [Gao et al. \(2019\)](#) introduced a two-step approach for reducing the HDFTS into a small number of latent factors with corresponding factor loadings and basis functions. To obtain a global FPCA projection for multi-population FTS, [Tavakoli et al. \(2023\)](#) arranged HDFTS into a panel structure and performed an eigendecomposition to the stacked FTS. [Zhou and Dette \(2023\)](#) derived Gaussian and multiplier bootstrap approximations for sums of HDFTS.

Parallel to the functional framework but still focusing on multi-population data, [Wang et al. \(2019\)](#) proposed a factor model for matrix-valued high-dimensional time series. Viewing the matrix input across columns and rows reveals information on dependence from two distinct perspectives. In the context of multi-population mortality data, all the considered ages can be arranged as row variables, whereas labels of the specific populations can be used as column variables. The model uses the mortality observations in any particular year to fill in the cells of the corresponding matrix and repeats the process for each observation time to form a matrix-valued time series. The correlation of mortality rates in the age direction and among the cross-sectional units can then be summarized via factor analysis into low-dimensional front-loading and back-loading matrices. All temporal information of the original data is retained in a low-dimensional matrix-values time series in the middle of the two loading matrices. This method developed by [Wang et al. \(2019\)](#) is conceptually similar to our dual-factor structure for HDFTS, introduced in Section 3, but considers conventional discrete-valued time series data.

Our proposed model has several advantages over the existing methods.

- 1) Our dual-factor model for HDFTS considers mortality observations as finite realizations of an underlying continuous process with age as a continuum. Under this functional framework, we can better capture mortality dependence across various ages for a particular population than can the matrix-valued time series factor model of [Wang et al. \(2019\)](#).

- 2) Compared to existing models for HDFTS, our proposed two-fold dimension reduction

algorithm can effectively isolate the homogeneous features for all data and the heterogeneous basis functions specific to each population, with the majority of the temporal dependence of the original HDFTS retained in a series of low-dimensional factor matrices. This separation of homogeneity and heterogeneity in HDFTS results in accurate forecasts for multi-population mortality data. On the one hand, the heterogeneous basis functions accommodate the unique characteristics of each population, reducing information loss in dimensionality reduction. On the other hand, the extracted homogenous features contribute to non-divergent forecasts for closely related populations.

3) We employ the dynamic FPCA for dimensionality reduction to adequately capture the temporal dependence of HDFTS (see, e.g., [Hörmann et al., 2015](#); [Rice and Shang, 2017](#)). This ideal property of dynamic FPCA is the result of using a long-run covariance function to estimate functional loadings. To our knowledge, the dynamic FPCA is often the preferred FTS feature extraction method for forecasting purposes ([Gao et al., 2019](#); [Yang et al., 2022](#)).

4) Our proposed model is highly flexible such that it can be viewed as a general case of several existing models by [Di et al. \(2009\)](#), [Gao et al. \(2019\)](#) and [Tavakoli et al. \(2023\)](#). By specifying appropriate front- and back-loading functions, our model can be reduced to these popular multi-population FTS models.

[Chang et al. \(2024\)](#) recently proposed a two-step procedure for modelling high-dimensional HDFTS (TSHDFTS) that initially performs independent component analysis of functional observations to achieve segmentations. Any two curves after transformation are uncorrelated, both cross-sectionally and temporally. The second step involves a latent decomposition to identify a finite-dimensional dynamic representation for each transformed curve. This modelling framework by [Chang et al. \(2024\)](#) may be viewed as a reduced form of (3.4) where the front-loading function is simplified to a constant matrix. Information loss is inevitable in this step of reducing functions to scalars. In contrast, our proposed dual-factor model can better capture the age-varying features of mortality rates via the front-loading functional factor. The empirical results in Section 7 verify that our proposed method produces more accurate point and interval forecasts than TSHDFTS.

[Jiménez-Varón et al. \(2024\)](#) considered a two-way functional ANOVA model for HDFTS that decomposes observations into a deterministic component capturing differences of the functional means and a time-varying residual component gauging the dynamic structure of the curves. Compared to the two-way functional ANOVA method, our proposed dual-factor model has a more flexible form, imposing fewer constraints on the functional means. Moreover, our dual-factor

model facilitates a decomposition of time-varying functional observations into common factors and their associated back-loading functions. The back-loading functions improve the interpretability of our results, while the common factors summarize time trends in human mortality functions.

The rest of the paper is organized as follows. Section 3 details our factor model and draws connections with several existing models. Section 4 outlines our estimation procedures. Section 5 describes our forecasting method based on the factor model for HDFTS. Section 6 presents Monte-Carlo simulation studies to show the finite-sample performance of the proposed method on recovering the homogeneous and heterogeneous features of HDFTS. Section 7 presents an empirical analysis of the Japanese subnational age-specific mortality data. Section 8 concludes the paper, highlighting how the methodology can be extended.

3 Factor model for HDFTS

We propose a new dual-factor model for HDFTS, which separates the homogeneity and heterogeneity within HDFTS. The homogeneity represents the similarity that is shared among all cross sections, while the heterogeneity represents the dissimilarity. In doing so, we reduce the dimensions of the HDFTS, including summarizing the temporal information of the original data into a low-dimensional matrix-valued time series. Doing so addresses the curse of dimensionality and makes forecasting feasible.

3.1 Functional panel data structure

Let $\{\mathcal{X}_t : t = 1, \dots, T\}$ be an N -dimensional FTS, where N is the number of sets of FTS, and T is the sample size or the number of functions within each set of FTS. The HDFTS can be organized into a single matrix format such that

$$\mathcal{X}(u) = \begin{bmatrix} \mathcal{X}_1^{(1)}(u) & \mathcal{X}_1^{(2)}(u) & \dots & \mathcal{X}_1^{(N)}(u) \\ \mathcal{X}_2^{(1)}(u) & \mathcal{X}_2^{(2)}(u) & \dots & \mathcal{X}_2^{(N)}(u) \\ \vdots & \vdots & \ddots & \vdots \\ \mathcal{X}_{T-1}^{(1)}(u) & \mathcal{X}_{T-1}^{(2)}(u) & \dots & \mathcal{X}_{T-1}^{(N)}(u) \\ \mathcal{X}_T^{(1)}(u) & \mathcal{X}_T^{(2)}(u) & \dots & \mathcal{X}_T^{(N)}(u) \end{bmatrix},$$

where $\mathcal{X}(u)$ is a $T \times N$ matrix, each entry in the matrix, $\mathcal{X}_t^{(i)}$ for $i \in \{1, \dots, N\}$, is defined in $\mathcal{H} := \mathcal{L}^2(\mathcal{I})$, a Hilbert space of square-integrable functions on a real interval $\mathcal{I} \in [a, b]$, with the inner product $\langle f, g \rangle = \int_{\mathcal{I}} f(u)g(u)$ and the norm $\|\cdot\| = \langle \cdot, \cdot \rangle^{\frac{1}{2}}$.

Under our setting, the i^{th} column of $\mathcal{X}(u)$, $\mathcal{X}^{(i)}(u) = [\mathcal{X}_1^{(i)}(u), \dots, \mathcal{X}_T^{(i)}(u)]^\top$, represents a FTS, which contains serial dependence. The t^{th} row of $\mathcal{X}(u)$, $\mathcal{X}_t(u) = [\mathcal{X}_t^{(1)}(u), \dots, \mathcal{X}_t^{(N)}(u)]$, consists of functions of all cross sections N at a specific time t . It is noteworthy that these are correlated. Let us consider the age-specific mortality rate as an example, each entry in $\mathcal{X}(u)$ represents the age-specific mortality rate curve of a specific region at a specific time. The i^{th} column of $\mathcal{X}(u)$ represents the mortality rate curves of region i across the sample period, and the t^{th} row of $\mathcal{X}(u)$ represents the mortality rate curves of all countries at time t .

3.2 Model setup

Denote $\mathcal{Y}_t^{(i)}(u) = \mathcal{X}_t^{(i)}(u) - \mu^{(i)}(u)$ as the centered FTS. Let us consider the following factor model for the centred HDFTS

$$(3.1) \quad \mathcal{Y}_t^{(i)}(u) = \phi(u) \mathbf{F}_t [\boldsymbol{\lambda}^{(i)}(u)]^\top + \epsilon_t^{(i)}(u),$$

where $\phi(u)$ is a vector of length r , with each entry being function-valued, that is, the features common to all sets of FTS; \mathbf{F}_t is an $r \times k$ matrix; $\boldsymbol{\lambda}^{(i)}(u)$ is a vector of length k , with each entry being function-valued, that is, specific for each $i \in \{1, 2, \dots, N\}$, which reflects the specific characteristic (heterogeneity) of each FTS; and $\epsilon_t^{(i)}(u)$ is a white noise idiosyncratic process that has no serial dependence (see, e.g., [Lam et al., 2011](#); [Lam and Yao, 2012](#)). We term $\phi(u)$ and $\boldsymbol{\lambda}^{(i)}(u)$ as front-loading and back-loading, respectively (see also [Wang et al., 2019](#)). The difference is that the factor loadings are scalar-valued in their work, while in our proposed model the factor loadings are function-valued. This extension allows our model to be more general.

3.3 Model interpretation

The proposed model can be interpreted in the following ways. We use the back-loadings to characterize the heterogeneity of the cross sections. Separating the heterogeneity reduces the original data into a multivariate FTS of smaller dimensions. These common multivariate FTS characterize the homogeneity of the original data. After reducing the dimensions of these common

multivariate FTS, the temporal information is captured by low-dimensional matrix-valued time series, which facilitates forecasting.

3.3.1 Dimension reduction along cross sections

Denoting $\mathcal{F}_t^\top(u) = \phi(u)\mathbf{F}_t$, then the model in (3.1) can be expressed as

$$(3.2) \quad \mathcal{Y}_t^{(i)}(u) = \boldsymbol{\lambda}^{(i)}(u)\mathcal{F}_t(u) + \epsilon_t^{(i)}(u),$$

where $\boldsymbol{\lambda}^{(i)}(u)$ is a k -dimensional functional factor loading vector, $\boldsymbol{\lambda}^{(i)}(u) = [\lambda_1^{(i)}(u), \dots, \lambda_k^{(i)}(u)]$, with each entry being a function, defined previously, and $\mathcal{F}_t(u)$ is a $k \times 1$ vector of functional factors at time t . This model differs from that of [Tavakoli et al. \(2023\)](#), where the factor loading is function-valued, and the factors are scalar. The front-loading $\boldsymbol{\lambda}^{(i)}(u)$ is dependent on i , which represents the heterogeneity of each FTS, while the functional factor $\mathcal{F}_t(u)$ is common to all i , which represents the common features of the HDFTS. Then, $\mathcal{F}(u) = [\mathcal{F}_1(u), \dots, \mathcal{F}_T(u)]^\top$ is a k -dimensional FTS ($k \ll N$). By doing this, we separate the common features of the HDFTS, denoted by $\mathcal{F}(u)$, from the heterogeneity, denoted by $\boldsymbol{\lambda}^{(i)}(u)$, and reduce the HDFTS to FTS with fewer dimensions.

[Bai \(2009\)](#) proposed a panel data model with interactive fixed effects, where the multiplication of the r -dimensional factor back-loading $\boldsymbol{\lambda}_i$ and common factors \mathbf{F}_t can be viewed as the interaction of these two terms. The interactive effects model is more general than the additive effects model. It allows the individual effect of i and the time effect of t to be involved in the model interactively rather than additively, giving more flexibility. [Freyberger \(2018\)](#) argued that the interactive fixed effects model could handle cases where heterogeneity is not time-homogeneous. [Tang et al. \(2022\)](#) proposed a functional panel data model with additive fixed effects. To handle time-varying heterogeneity, they further proposed a clustering algorithm to search for homogeneous subgroups before jointly modelling the FTS. Our model can be viewed as a functional extension of the interactive fixed-effects model, as stated in (3.2), where both the factor loading $\boldsymbol{\lambda}^{(i)}(u)$ and the common factors $\mathcal{F}_t(u)$ are function-valued, and $\boldsymbol{\lambda}^{(i)}(u)$ captures the specific effects of different cross sections and $\mathcal{F}_t(u)$ denotes the common features with the multiplication of $\boldsymbol{\lambda}^{(i)}(u)$ and $\mathcal{F}_t(u)$ allowing for time-varying heterogeneity.

3.3.2 Dimension reduction on infinite-dimensional functions

After applying dimension reduction, the FTS $\mathcal{F}_t^\top(u)$ are obtained. Then, a functional factor model can be applied such that

$$(3.3) \quad \mathcal{F}_t^\top(u) = \phi(u)\mathbf{F}_t + \mathbf{v}_t(u),$$

where $\phi(u)$, the common functional loading, is a vector of length r ; \mathbf{F}_t is an $r \times k$ matrix and $\mathbf{v}_t(u)$ is also the white noise idiosyncratic component. In doing so, all the temporal dynamics are reflected in the matrix-valued time series $\{\mathbf{F}_t\}$.

Combining (3.2) and (3.3), we can obtain the proposed model as in (3.1). The HDFTS $\mathcal{Y}_t(u) = [\mathcal{Y}_t^1(u), \dots, \mathcal{Y}_t^N(u)]^\top$ can also be expressed in a matrix format,

$$(3.4) \quad \mathcal{Y}_t(u) = \phi(u)\mathbf{F}_t[\Lambda(u)]^\top + \epsilon_t(u),$$

where the systems of back-loadings $\Lambda(u) = [\Lambda^{(1)}(u), \dots, \Lambda^{(N)}(u)]$ are an $(N \times k, k \ll N)$ matrix, with the i^{th} row being $\lambda^{(i)}(u)$; and $\epsilon_t(u)$ is an N -dimensional vector of the white noise processes.

To better understand the model, we can extend the first component on the right-hand side of (3.4) as

$$(3.5) \quad \begin{aligned} \phi(u)\mathbf{F}_t[\Lambda(u)]^\top &= \begin{bmatrix} \phi_1(u) & \phi_2(u) & \dots & \phi_r(u) \end{bmatrix} \begin{bmatrix} F_{t,11} & F_{t,12} & \dots & F_{t,1k} \\ F_{t,21} & F_{t,22} & \dots & F_{t,2k} \\ \vdots & \vdots & \ddots & \vdots \\ F_{t,r1} & F_{t,r2} & \dots & F_{t,rk} \end{bmatrix} \begin{bmatrix} \lambda_1^{(1)}(u) & \lambda_1^{(2)}(u) & \dots & \lambda_1^{(N)}(u) \\ \lambda_2^{(1)}(u) & \lambda_2^{(2)}(u) & \dots & \lambda_2^{(N)}(u) \\ \vdots & \vdots & \ddots & \vdots \\ \lambda_k^{(1)}(u) & \lambda_k^{(2)}(u) & \dots & \lambda_k^{(N)}(u) \end{bmatrix} \\ &= \left[\sum_{p=1}^r \sum_{q=1}^k \phi_p(u)F_{t,pq}\lambda_q^{(1)}(u) \quad \sum_{p=1}^r \sum_{q=1}^k \phi_p(u)F_{t,pq}\lambda_q^{(2)}(u) \quad \dots \quad \sum_{p=1}^r \sum_{q=1}^k \phi_p(u)F_{t,pq}\lambda_q^{(N)}(u) \right] \end{aligned}$$

where $\phi(u)$ is the loading functions common to all cross sections. $\Lambda(u)$ is the system loading curves specific to different cross sections. By reducing the dimensions of both functional continuum and cross sections, we can extract the important information of the HDFTS into an $r \times k \times T$ factor array \mathbf{F} . This array forms a matrix-valued time series, $\{\mathbf{F}_t, t = 1, 2, \dots, T\}$, which contains all the temporal dynamics of the HDFTS.

3.3.3 Connections with other existing models

The generality of the proposed model lies in the flexibility of the choice of the front- and back-loading functions. The connections with other existing models are discussed here.

Case 1 (Additive Fixed-Effect Model, Di et al. (2009)): Setting each entry in the back-loading being the same constant function, that is, $\lambda_q^{(i)}(u) = c$ for all $q \in 1, 2, \dots, k$ and $i \in 1, 2, \dots, N$. Equation (3.5) can be reduced as

$$\phi(u) \mathbf{F}_t \mathbf{\Lambda}^\top(u) = \left[\sum_{p=1}^r \phi_p(u) \sum_{q=1}^k c F_{t,pq} \quad \sum_{p=1}^r \phi_p(u) \sum_{q=1}^k c F_{t,pq} \quad \dots \quad \sum_{p=1}^r \phi_p(u) \sum_{q=1}^k c F_{t,pq} \right]$$

Let $\beta_{t,p} = \sum_{q=1}^k c F_{t,pq}$, then $\mathcal{X}_t^{(i)}(u)$ can be expressed as

$$\mathcal{X}_t^{(i)}(u) = \mu^{(i)}(u) + \sum_{p=1}^r \beta_{t,p} \phi_p(u) + E_t^{(i)}(u),$$

where $E_t^{(i)}(u)$ is the error component, for ease of notation, let $E_t^{(i)}(u)$ represent the error component for different models described below. This is the special case of a functional panel data model with additive fixed effects as in Di et al. (2009), where there is no component for the cross section, i .

Case 2 (Multivariate FPCA): If we set each entry in the back-loading matrix as a constant function specific to each i , i.e., $\lambda_q^{(i)}(u) = c_i$, for all $q \in 1, 2, \dots, k$. Equation (3.5) can be reduced as

$$\phi(u) \mathbf{F}_t \mathbf{\Lambda}^\top(u) = \left[\sum_{p=1}^r \phi_p(u) \sum_{q=1}^k c_1 F_{t,pq} \quad \sum_{p=1}^r \phi_p(u) \sum_{q=1}^k c_2 F_{t,pq} \quad \dots \quad \sum_{p=1}^r \phi_p(u) \sum_{q=1}^k c_N F_{t,pq} \right]$$

Let $\beta_{t,p}^{(i)} = \sum_{q=1}^k c_i F_{t,pq}$, then $\mathcal{X}_t^{(i)}(u)$ can be expressed as

$$\mathcal{X}_t^{(i)}(u) = \mu^{(i)}(u) + \sum_{p=1}^r \beta_{t,p}^{(i)} \phi_p(u) + E_t^{(i)}(u), \quad t = 1, 2, \dots, T,$$

then the model becomes the Karhunen-Loève representation for multivariate functional data, where all functions from different cross sections share the same bases.

Case 3 (High-Dimensional Factor Model, Tavakoli et al. (2023)): If we set each entry in the back-loading matrix as a function specific to i , that is, $\lambda_q^{(i)}(u) = \gamma^{(i)}(u)$, for all $q \in 1, 2, \dots, k$.

Equation (3.5) can be reduced as

$$\phi(u)\mathbf{F}_t\boldsymbol{\Lambda}^\top(u) = \left[\sum_{p=1}^r \gamma^{(1)}(u)\phi_p(u) \sum_{q=1}^k F_{t,pq} \quad \sum_{p=1}^r \gamma^{(2)}(u)\phi_p(u) \sum_{q=1}^k F_{t,pq} \quad \dots \quad \sum_{p=1}^r \gamma^{(N)}(u)\phi_p(u) \sum_{q=1}^k F_{t,pq} \right]$$

Let $\beta_{t,p} = \sum_{q=1}^k F_{t,pq}$ and $\phi_p^{(i)}(u) = \gamma^{(i)}(u)\phi_p(u)$, $\mathcal{X}_t^{(i)}(u)$ can be expressed as

$$\mathcal{X}_t^{(i)}(u) = \mu^{(i)}(u) + \sum_{p=1}^r \beta_{t,p} \phi_p^{(i)}(u) + E_t^{(i)}(u), \quad t = 1, 2, \dots, T,$$

then it is the high-dimensional factor model of [Tavakoli et al. \(2023\)](#). Similarly, we can obtain the same model if the front-loading is set to be a constant scalar, i.e., $\phi_p(u) = c$.

Case 4 (Individual FPCA, [Gao et al. \(2019\)](#)): If we set each entry in the front-loading being a constant specific to i for $i = 1, 2, \dots, N$, that is, $\phi_p(u) = c_i$ for all $p = 1, 2, \dots, r$. Equation (3.5) can be re-expressed as

$$\phi(u)\mathbf{F}_t\boldsymbol{\Lambda}^\top(u) = \left[\sum_{q=1}^k \lambda_q^{(1)}(u) \sum_{p=1}^r c_1 F_{t,pq} \quad \sum_{q=1}^k \lambda_q^{(2)}(u) \sum_{p=1}^r c_2 F_{t,pq} \quad \dots \quad \sum_{q=1}^k \lambda_q^{(N)}(u) \sum_{p=1}^r c_N F_{t,pq} \right]$$

Let $\beta_{t,q}^{(i)} = \sum_{p=1}^r c_i F_{t,pq}$ and $\phi_q^{(i)}(u) = \lambda_q^{(i)}(u)$, $\mathcal{X}_t^{(i)}(u)$ can be expressed as

$$\mathcal{X}_t^{(i)}(u) = \mu^{(i)}(u) + \sum_{q=1}^k \beta_{t,q}^{(i)} \phi_q^{(i)}(u) + E_t^{(i)}(u), \quad t = 1, 2, \dots, T,$$

then it is the Karhunen-Loève representation for univariate functional data, from which the factor model of [Gao et al. \(2019\)](#) is derived.

Case 5 (Matrix Factor Model, [Wang et al. \(2019\)](#)): If we discretize the functional continuum u into grid points and consider the discrete high-dimensional setting rather than the functional setting, and set each entry in the back-loading matrix is a different scalar, that is, $\lambda_q^{(i)}(u) = c_{i,q}$, then it is equivalent to the factor model for high-dimensional matrix-valued time series of [Wang et al. \(2019\)](#).

4 Parameter estimation

We present an estimation procedure for parameters $\{\mu^{(i)}(u), \phi(u), \mathbf{F}_t\}$ in (3.1). In general, the idea of the estimation procedure is to estimate the systems of back-loading first so that the HDFTS is

reduced to the FTS of lower dimensions. We then proceed to estimate the common front-loading and the matrix-valued time series, F_t .

Suppose we have T curves in each cross section, the estimation of $\mu^{(i)}(u)$ is as follows

$$\widehat{\mu}^{(i)}(u) = \frac{1}{T} \sum_{t=1}^T \mathcal{X}_t^{(i)}(u).$$

Then, $\mathcal{Y}_t^{(i)}(u)$ is expressed as

$$\mathcal{Y}_t^{(i)}(u) = \mathcal{X}_t^{(i)}(u) - \widehat{\mu}^{(i)}(u).$$

4.1 Estimation of functional loadings $\Lambda(u)$

The cross-sectional specific functional back-loadings $\{\lambda^{(i)}(u)\}$ represent the heterogeneity of each FTS. To accommodate the serial dependence in each cross section, $\lambda^{(i)}(u)$ is estimated by the eigendecomposition of the long-run covariance operator corresponding to the i^{th} cross section.

Given the inadequacy of classic FPCA in accounting for the essential information provided by the serial dependence structure in FTS, dynamic FPCA is developed. [Horváth et al. \(2013\)](#) and [Panaretos and Tavakoli \(2013\)](#) defined smoothed periodogram-type estimates of the long-run covariance and spectral density operators for FTS. [Hörmann et al. \(2015\)](#) used the spectral density operator to create functional filters to construct mutually uncorrelated dynamic FPCs so that the dynamic FPC scores can be analyzed component-wise. [Rice and Shang \(2017\)](#) proposed a bandwidth selection method for estimates of the long-run covariance function based on finite-order weight functions that aim to minimize the estimator's asymptotic mean-squared normed error. Following their work, the long-run covariance function for the i^{th} cross section $c^{(i)}(u, v)$ can be estimated by

$$\widehat{c}^{(i)}(u, v) = \sum_{s=-\infty}^{\infty} W\left(\frac{s}{h}\right) \widehat{c}_s^{(i)}(u, v),$$

where

$$\widehat{c}_s^{(i)}(u, v) = \begin{cases} \frac{1}{T-s} \sum_{t=1}^{T-s} \widehat{\mathcal{Y}}_t^{(i)}(u) \widehat{\mathcal{Y}}_{t+s}^{(i)}(v), & s \geq 0; \\ \frac{1}{T-s} \sum_{t=1-s}^T \widehat{\mathcal{Y}}_t^{(i)}(u) \widehat{\mathcal{Y}}_{t+s}^{(i)}(v), & s < 0. \end{cases}$$

$W(\cdot)$ is the kernel function that assigns different weights to the auto-covariance functions of different lags, and h is the bandwidth. Despite many different types of kernel functions (see

Hansen, 1982; White, 1984; Newey and West, 1987; Andrews, 1991; Gallant, 2009, for types of kernel functions), it is common to assign more weight to the auto-covariance functions of small lags and less weight to the auto-covariance functions of large lags. Here, we use flat-top kernel functions as they give a reduced bias and faster rates of convergence (Politis and Romano, 1996, 1999). Flat-top kernels are of the following form

$$W\left(\frac{s}{h}\right) = \begin{cases} 1, & 0 \leq \left|\frac{s}{h}\right| < m; \\ \frac{\left|\frac{s}{h}\right|-1}{m-1}, & m \leq \left|\frac{s}{h}\right| < 1; \\ 0, & \left|\frac{s}{h}\right| \geq 1, \end{cases}$$

where $m < 1$. The choice of bandwidth can greatly affect the finite-sample performance. Therefore, we apply the adaptive bandwidth selection procedure of Rice and Shang (2017) to gain a better estimate of the long-run covariance functions.

The long-run covariance operator can be estimated by

$$\widehat{C}^{(i)}(y)(u) = \sum_{s=-\infty}^{\infty} W\left(\frac{s}{h}\right) \widehat{C}_s^{(i)}(y)(u),$$

where $\widehat{C}_s^{(i)}(y)(u) = \int_{\mathcal{I}} \widehat{c}_s^{(i)}(u, v) y(v) dv$, is the sample covariance operator at lag s .

The estimates of $\lambda^{(i)}(u)$, denoted by $\widehat{\lambda}^{(i)}(u) = [\widehat{\lambda}_1^{(i)}(u), \dots, \widehat{\lambda}_{k_i}^{(i)}(u)]$, are the eigenfunctions corresponding to the first k_i largest eigenvalues of $\widehat{C}^{(i)}(y)(u)$. Since we allow the $\lambda^{(i)}(u)$ to vary according to i , it represents the heterogeneity of each population.

To maintain the matrix format of the loadings of each population, k is selected to be

$$k = \max\{k_i : 1 \leq i \leq N\},$$

where k_i is the retained number of components used for i^{th} population.

The selection of the optimal number of functional principal components has been studied widely in the literature (Rice and Silverman, 1991; Yao et al., 2005; Hall and Vial, 2006; Chiou, 2012; Hörmann and Kidziński, 2015). In this paper, k_i is determined by the cumulative percentage of variance method (Chiou, 2012), such that

$$(4.6) \quad k_i = \operatorname{argmin}_{k_i: k_i \geq 1} \left\{ \frac{\sum_{m=1}^{k_i} \widehat{\lambda}_m^{(i)}}{\sum_{m=1}^{\infty} \widehat{\lambda}_m^{(i)} \mathbb{1}\{\widehat{\lambda}_m^{(i)} > 0\}} \geq P \right\},$$

where $\lambda_m^{(i)}$ is the m^{th} largest eigenvalue of $\widehat{C}^{(i)}(y)(u)$, $\mathbb{1}\{\cdot\}$ denotes the binary indicator function and P is a pre-determined value and is chosen to be 0.9 (see, e.g., [Horváth and Kokoszka, 2012](#)).

4.2 Estimation of $\mathcal{F}_t(u)$

In order to estimate $\phi(u)$ and F_t , we need to estimate $\mathcal{F}_t(u)$ in (3.2), that is, extract the common features of the HDFTS. Expressing (3.2) in matrix format,

$$\mathcal{Y}_t(u) = \Lambda(u)\mathcal{F}_t(u) + \epsilon_t(u),$$

where $\Lambda(u)$ is an $N \times k$ matrix of functions and $\mathcal{F}_t(u)$ is a $k \times 1$ vector of functions. The i^{th} entry of $\mathcal{Y}_t(u)$ can be expressed as follows:

$$\mathcal{Y}_t^{(i)}(u) = \sum_{q=1}^k \lambda_q^{(i)}(u)\mathcal{F}_{t,q}(u) + \epsilon_t^{(i)}(u).$$

This is essentially the functional concurrent regression model in [Ramsay et al. \(2009\)](#), but without intercept function, where $\lambda_q^{(i)}(u)$ is a k -dimensional functional observation and $\mathcal{F}_{t,q}(u)$ is the functional regression coefficients.

Let the N -dimensional residual functions vector be

$$\mathbf{r}_t(u) = \mathcal{Y}_t(u) - \Lambda(u)\mathcal{F}_t(u),$$

then $\mathcal{F}_t(u)$ can be estimated by minimizing the penalized sum of squares, such that

$$(4.7) \quad \widehat{\mathcal{F}}_t(u) = \underset{\mathcal{F}_t(u)}{\operatorname{argmin}} \left(\int_{\mathcal{I}} \mathbf{r}_t^\top(u) \mathbf{r}_t(u) du + \sum_{q=1}^k \gamma_q \int_{\mathcal{I}} [L_q \mathcal{F}_{t,q}(u)]^2 du \right),$$

where γ_q is the smoothing parameter and $L_q \mathcal{F}_{t,q}(u)$ is the linear differential operator applied to $\mathcal{F}_{t,q}(u)$. Together, γ_q and $L_q \mathcal{F}_{t,q}(u)$ define the roughness penalty.

Functional concurrent regression is performed for each $t = 1, 2, \dots, T$, such that $\widehat{\mathcal{F}}(u) = [\widehat{\mathcal{F}}_1(u)^\top, \widehat{\mathcal{F}}_2(u)^\top, \dots, \widehat{\mathcal{F}}_T(u)^\top]^\top$ is a matrix of function-valued objects, each with a dimension of $T \times k$, so that we have a panel of dimension-reduced FTS, which represents the common features.

4.3 Estimation of the front-loading function $\phi(u)$ and factor matrix F_t

Once $\widehat{\mathcal{F}}(u)$ is obtained, we can estimate $\phi(u)$ and F_t based on (3.3). Since $\mathcal{F}(u)$ is a dimension-reduced panel of FTS, where each column may be correlated, the key is to calculate the auto-cross-covariance of $\mathcal{F}(u)$. Wang et al. (2019) used the auto-cross-covariance to capture the co-movement observations from different cross sections of different lags. We extend it to the functional setting. Let $C_{h,lj}(u, v)$ be the auto-cross-covariance function of the l^{th} and j^{th} column of $\mathcal{F}(u)$, for l and $j = 1, \dots, k$, such that

$$C_{h,lj}(u, v) = \text{Cov} \left[\mathcal{F}_{t,l}(u), \mathcal{F}_{t+h,j}(u) \right].$$

Since the operator using $C_{h,lj}(u, v)$ as a kernel is not nonnegative, we define a nonnegative operator (using a similar idea as Bathia et al., 2010),

$$M_{h,lj}(u, v) = \int_{\mathcal{I}} C_{h,lj}(u, z) C_{h,lj}(v, z) dz.$$

For a pre-determined integer h_0 , the operator

$$(4.8) \quad M(u, v) = \sum_{h=1}^{h_0} \sum_{l=1}^k \sum_{j=1}^k M_{h,lj}(u, v),$$

is also nonnegative. The auto-cross-covariance function can be estimated by

$$\widehat{C}_{h,lj}(u, v) = \frac{1}{T-h} \sum_{t=1}^{T-h} \widehat{\mathcal{F}}_{t,l}(u) \widehat{\mathcal{F}}_{t+h,j}(v).$$

Hence, the operator $M(u, v)$ can be estimated by

$$\widehat{M}(u, v) = \sum_{h=1}^{h_0} \sum_{l=1}^k \sum_{j=1}^k \int_{\mathcal{I}} \widehat{C}_{h,lj}(u, z) \widehat{C}_{h,lj}(v, z) dz.$$

The estimates of $\phi(u)$, $\widehat{\phi}(u) = [\widehat{\phi}_1(u), \dots, \widehat{\phi}_r(u)]$, are the eigenfunctions corresponding to the first r largest eigenvalues of the eigen-decomposition on $\widehat{M}(u, v)$. The optimal r can be selected using the same approach as in (4.6).

Once $\widehat{\phi}(u)$ is obtained, the estimated \widehat{F}_t can be obtained through

$$\widehat{F}_t = \int_{\mathcal{I}} \widehat{\phi}(u)^\top \widehat{\mathcal{F}}_t(u)^\top du,$$

where $\widehat{\mathbf{F}}_t$ is an $r \times k$ matrix. Therefore, all the temporal information is extracted into the T sheets of $r \times k$ matrices.

In summary, we first separate the heterogeneity among the HDFTS, where a specific set of functional loading, $\widehat{\boldsymbol{\lambda}}^{(i)}(u)$, is obtained for each FTS. The common features can then be extracted into FTS of smaller dimensions, $\widehat{\mathcal{F}}_t(u)$. Then, the functional dynamic factor model is applied to the dimension-reduced FTS, $\widehat{\mathcal{F}}_t(u)$, such that all the temporal information can be extracted into the matrix-valued time series $\{\widehat{\mathbf{F}}_t : t = 1, \dots, T\}$.

5 Forecasting

Based on the proposed model, the functional panel data are extracted into T sheets of fixed-dimensional factor matrices, \mathbf{F}_t . Forecasting the HDFTS is equivalent to forecasting the estimated factor matrices, $\widehat{\mathbf{F}}_t$. The h -step-ahead in sample forecast of the estimated factors, $\widehat{\mathbf{F}}_{\kappa+h|\kappa}$ can be obtained by fitting a vector autoregressive (VAR) model to the estimated factors $\{\widehat{\mathbf{F}}_1, \widehat{\mathbf{F}}_2, \dots, \widehat{\mathbf{F}}_\kappa\}^\top$, where $\kappa < T$ is a sample size used for out-of-sample forecasting. In selecting the order of the VAR model, we follow the method of [Tsay \(2013\)](#), where an information criterion, such as the Akaike information criterion, is used.

For a given sample size κ , the h -step-ahead in-sample forecast of the i^{th} cross section in the HDFTS can be calculated as

$$\widehat{\mathcal{X}}_{\kappa+h|\kappa}^{(i)}(u) = \widehat{\boldsymbol{\mu}}^{(i)}(u) + \widehat{\boldsymbol{\phi}}(u)\widehat{\mathbf{F}}_{\kappa+h|\kappa}[\widehat{\boldsymbol{\lambda}}^{(i)}(u)]^\top.$$

To capture the uncertainties associated with the point forecasts, point-wise prediction intervals could also be constructed. We apply the nonparametric bootstrap approach of [Shang \(2018\)](#) in constructing point-wise prediction intervals.

For a grid point u_j on the curve, the h -step-ahead bootstrapped forecasts of the i^{th} cross section, $\widehat{\mathcal{X}}_{\kappa+h|\kappa}^{(i),b}(u_j)$, can be obtained by adding a bootstrapped residual, $\widehat{e}_{\kappa+h|\kappa}^{(i),b}(u_j)$ to the point forecast, $\widehat{\mathcal{X}}_{\kappa+h|\kappa}^{(i)}(u_j)$. The $\widehat{e}_{\kappa+h|\kappa}^{(i),b}(u_j)$ is generated using sampling with replacement from the in-sample forecast errors,

$$\widehat{e}_{\delta+h|\delta}^{(i)}(u_j) = \mathcal{X}_{\delta+h}^{(i)}(u_j) - \widehat{\mathcal{X}}_{\delta+h|\delta}^{(i)}(u_j), \quad \delta = 2, \dots, T - h.$$

For a given significance level α , the h -step-ahead bootstrapped point-wise prediction interval for

the i^{th} cross section, $[\widehat{\mathcal{X}}_{\kappa+h|\kappa}^{(i),\text{lb}}(u_j), \widehat{\mathcal{X}}_{\kappa+h|\kappa}^{(i),\text{ub}}(u_j)]$, can be calculated point-wise as the $100 \times (\alpha/2)^{\text{th}}$ and $100 \times (1 - \alpha/2)^{\text{th}}$ percentile of the bootstrapped forecasts at each grid point, respectively. The estimation procedure and the forecasting method are summarized in Algorithm 1.

Algorithm 1: HDFTS forecasting

1 **Input:** HDFTS $\{\mathbf{X}_t(u) = [\mathcal{X}_t^{(1)}, \mathcal{X}_t^{(2)}, \dots, \mathcal{X}_t^{(N)}], t = 1, \dots, \kappa\}$.

2 **Estimation Step:**

2.1 For $i \in \{1, \dots, N\}$, compute the sample mean $\widehat{\mu}^{(i)} = \frac{1}{\kappa} \sum_{t=1}^{\kappa} \mathcal{X}_t^{(i)}(u)$;

2.2 For $i \in \{1, \dots, N\}$, compute the demeaned function $\widehat{\mathcal{Y}}_t^{(i)} = \mathcal{X}_t^{(i)}(u) - \widehat{\mu}^{(i)}$;

2.3 For $i \in \{1, \dots, N\}$, perform dynamic FPCA to $\widehat{\mathcal{Y}}^{(i)} = [\widehat{\mathcal{Y}}_1^{(i)}, \widehat{\mathcal{Y}}_2^{(i)}, \dots, \widehat{\mathcal{Y}}_{\kappa}^{(i)}]^{\top}$ and obtain the eigenfunctions $\widehat{\lambda}^{(i)}(\mathbf{u}) = [\widehat{\lambda}_1^{(i)}(\mathbf{u}), \dots, \widehat{\lambda}_{k_i}^{(i)}(\mathbf{u})]$ corresponding to the first k_i largest eigenvalues of the long-run covariance operator of $\widehat{\mathcal{Y}}_t^{(i)}$, where k_i is selected based on (4.6);

2.4 Choose $k = \max\{k_i : 1 \leq i \leq N\}$, such that the loadings of each cross section are of the same dimension such that $\Lambda(\mathbf{u}) = [\widehat{\lambda}^{(1)}(\mathbf{u}), \widehat{\lambda}^{(2)}(\mathbf{u}), \dots, \widehat{\lambda}^{(N)}(\mathbf{u})]^{\top}$;

2.5 For $t \in \{1, \dots, \kappa\}$, perform the concurrent functional regression with $\{\widehat{\mathcal{Y}}_t^{(i)}, i = 1, \dots, N\}$ as the response and $\{\widehat{\lambda}^{(i)}(\mathbf{u}), i = 1, \dots, N\}$ as covariates and obtain the coefficient functions $\widehat{\mathcal{F}}_t(u) = [\widehat{\mathcal{F}}_{t,1}(u), \dots, \widehat{\mathcal{F}}_{t,k}(u)]$ and $\widehat{\mathcal{F}}(u) = [\widehat{\mathcal{F}}_1(u)^{\top}, \widehat{\mathcal{F}}_2(u)^{\top}, \dots, \widehat{\mathcal{F}}_T(u)^{\top}]^{\top}$;

2.6 For $i, j \in \{1, \dots, k\}$, compute $\widehat{C}_{h,lj}(u, v) = \frac{1}{T-h} \sum_{t=1}^{T-h} \widehat{\mathcal{F}}_{t,l}(u) \widehat{\mathcal{F}}_{t+h,j}(v)$;

2.7 For a predetermined h_0 , compute $\widehat{M}(u, v) = \sum_{h=1}^{h_0} \sum_{l=1}^k \sum_{j=1}^k \int_{\mathcal{I}} \widehat{C}_{h,lj}(u, z) \widehat{C}_{h,lj}(v, z) dz$;

2.8 Conduct eigendecomposition on $\widehat{M}(u, v)$ and get $\widehat{\phi}(u) = [\widehat{\phi}_1(u), \dots, \widehat{\phi}_r(u)]$, the eigenfunctions corresponding to the first r largest eigenvalues of $\widehat{M}(u, v)$, where r is selected based on similar idea as in (4.6);

2.9 For $t \in \{1, \dots, \kappa\}$, compute $\widehat{\mathbf{F}}_t = \int \widehat{\phi}(u)^{\top} \widehat{\mathcal{F}}_t(u)^{\top} du$.

3. **Forecasting Step:**

3.1 Obtain the h -step ahead forecast of $\{\widehat{\mathbf{F}}_t, t = 1, \dots, \kappa\}$, $\widehat{\mathbf{F}}_{\kappa+h|\kappa}$;

3.2 Recover the h -step-ahead forecast of the i^{th} cross section of the HDFTS,
 $\widehat{\mathcal{X}}_{\kappa+h|\kappa}^{(i)}(u) = \widehat{\mu}^{(i)}(u) + \widehat{\phi}(u) \widehat{\mathbf{F}}_{\kappa+h|\kappa} \widehat{\lambda}^{(i)}(u)$.

Result: $\widehat{\mathcal{X}}_{\kappa+h|\kappa}^{(i)}(u)$, the h -step-ahead forecast of the i^{th} cross section of the HDFTS.

6 Simulation studies

We consider a series of Monte-Carlo simulations to evaluate the finite-sample performance of the proposed method. The data generating process (DGP) is designed to show the proposed method's ability to accurately recover the front factor loading $\phi(u)$ and the back factor loading $\lambda^{(i)}(u)$ of FTS.

1) The simulated $\{\mathcal{Y}_t^{(i)}(u)\}$ functions are highly positively correlated, corresponding to the

strong temporal correlation. This is achieved by adopting VAR models with positive-diagonal coefficient matrices.

- 2) The elements in the back factor loading $\boldsymbol{\lambda}^{(i)}(u)$ are designed to slightly vary according to $i = 1, \dots, N$.
- 3) The elements of front factor loading $\boldsymbol{\phi}(u)$ are selected to be independent of the individual index i . This setting is consistent with the practice that one set of homogenous basis functions is used in modelling highly correlated data.

In total, we generate N sets of correlated FTS according to (3.1). In particular, the t^{th} curve of the i^{th} FTS is generated from the following model contaminated with measurement error $\epsilon_t^{(i)}(u)$

$$\mathcal{Y}_t^{(i)}(u) = \boldsymbol{\phi}(u) \mathbf{F}_t [\boldsymbol{\lambda}^{(i)}(u)]^\top + \epsilon_t^{(i)}(u),$$

where \mathbf{F}_t is a 2×2 matrix with each row generated using a VAR model of order 1. Specifically, the first and second rows are generated using VAR(1) model with coefficient matrices

$$\begin{pmatrix} 0.7 & 0.2 \\ 0.2 & 0.7 \end{pmatrix}, \quad \begin{pmatrix} 0.5 & -0.25 \\ -1 & 0.5 \end{pmatrix}.$$

The covariance matrix of the innovations for both VAR(1) models are $\begin{pmatrix} 1 & 0.5 \\ 0.5 & 1 \end{pmatrix}$. The two front-loading curves are $\phi_1(u) = \sin(4\pi u)$ and $\phi_2(u) = \cos(4\pi u)$, respectively, with $\{u = \frac{m}{100} : m = 0, 1, \dots, 100\}$. The two back-loading curves for each i are $\lambda_2^{(i)} = \sin(2\pi u + i\pi/4)$ and $\lambda_1^{(i)} = \cos(2\pi u + i\pi/4)$, respectively. The measurement error $\epsilon_t^{(i)}(u)$ is generated from independent and identically distributed $\mathcal{N}(0, 0.5^2)$ for all i and u .

The considered DGP involves different combinations of N and T . We select a moderate size $T = 20, 40$ and choose N to equal $\frac{T}{2}$, T and $2T$. The pre-determined integer h_0 in (4.8) is taken to be one as the VAR(1) model is considered.

The in-sample model fitting can be evaluated using root mean squared error (RMSE)

$$\text{RMSE}(h) = \sqrt{\frac{1}{N \times T \times 101} \sum_{i=1}^N \sum_{t=1}^T \sum_{m=1}^{101} [\mathcal{Y}_t^{(i)}(u_m) - \widehat{\mathcal{Y}}_t^{(i)}(u_m)]^2},$$

where $\widehat{\mathcal{Y}}_t^{(i)}(u_m)$ represents the estimated function value at grid points $u_m \in [0, 1]$. For each

combination of N and T , we simulate 100 replications with pseudo-random seeds and compute the mean of the RMSE values.

Table 1 displays the model fitting performance. For each N , when T increases, the estimation error is smaller. For each T , as N increases, the estimation error is stable, and the proportion of the corrected estimated number of factors significantly increases, which indicates that our model can handle high-dimensional cases when $N > T$.

Table 1: Estimation performance for different combinations of N and T . RMSE measures the model fitting, and \hat{r} and \hat{k} measure the proportion of the correctly estimated number of front- and back-loading curves.

| T | N | RMSE | $\hat{r} = 2 \text{ or } 3$ | $\hat{k} = 2$ |
|-----|-----|------|-----------------------------|---------------|
| 40 | 20 | 1.12 | 0.66 | 0.93 |
| | 40 | 0.99 | 0.73 | 0.96 |
| | 80 | 1.07 | 0.82 | 0.98 |

We also compare the forecast performance of the proposed model with the univariate FTS forecasting method of Hyndman and Ullah (2007). The simulated data is split into two sets in evaluating the forecasting performance, that is, the training set and the testing set. Different models are fitted with the training dataset, and forecasts are made based on different models. Then, the forecasts are compared with the actual observations in the testing set. In this case, we set the starting size of the training set and testing set as $\frac{3}{4} \times T$ and $\frac{1}{4} \times T$, respectively. We use expanding window analysis, where we increase the training size in each iteration by one and refit the models. We obtain the one- to ten -step-ahead forecasts and compute our forecasts' root mean square forecast error (RMSFE).

$$\text{RMSFE}(h) = \sqrt{\frac{1}{N \times (\frac{1}{4} \times T - h + 1) \times 101} \sum_{i=1}^N \sum_{\kappa=\frac{3}{4} \times T}^{T-h} \sum_{m=1}^{101} [\mathcal{Y}_{\kappa+h}^{(i)}(u_m) - \hat{\mathcal{Y}}_{\kappa+h|\kappa}^{(i)}(u_m)]^2},$$

where κ is the size of the data used to generate forecast and $\hat{\mathcal{Y}}_{\kappa+h|\kappa}^{(i)}(u_m)$ represents the forecast values at grid points u_m .

For each combination of N and T , we simulate 100 replications and compute the mean of the RMSFE values of different models. Table 2 shows the mean RMSFE values for different combinations of N and T for both models. The bold entries highlight the method that produces the

most accurate forecast. The proposed model produces more accurate forecasts for most of the cases for all the combinations of N and T , demonstrating the proposed model’s superiority in forecasting HDFTS.

Table 2: *The mean of RMSFE values of different models for different combinations of N and T , “FDFM” represents the proposed model and “UFTS” represents the univariate FTS forecasting model.*

| T | h | $N = 20$ | | $N = 40$ | | $N = 80$ | |
|-----|-----|----------|--------------|----------|--------------|----------|--------------|
| | | UFTS | FDFM | UFTS | FDFM | UFTS | FDFM |
| 40 | 1 | 2.189 | 1.381 | 2.647 | 1.478 | 2.758 | 1.555 |
| | 2 | 2.276 | 1.661 | 2.743 | 1.862 | 2.856 | 1.958 |
| | 3 | 2.362 | 1.858 | 2.841 | 2.141 | 2.977 | 2.223 |
| | 4 | 2.447 | 2.091 | 2.956 | 2.301 | 3.008 | 2.356 |
| | 5 | 2.493 | 2.202 | 3.131 | 2.530 | 3.184 | 2.589 |

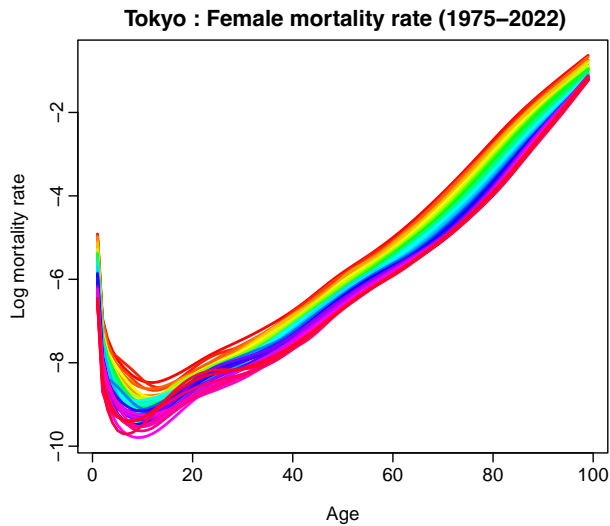
7 Empirical studies

We apply the proposed method to forecast sub-national mortality rates in Japan ([Japan Mortality Database, 2024](#)). In particular, we consider the age-specific mortality rates of 47 prefectures of Japan from 1975 to 2021. We pick this time interval to ensure the number of observation years is less than the number of prefectures, ensuring the “curse of dimensionality” challenges are preserved in the empirical data.

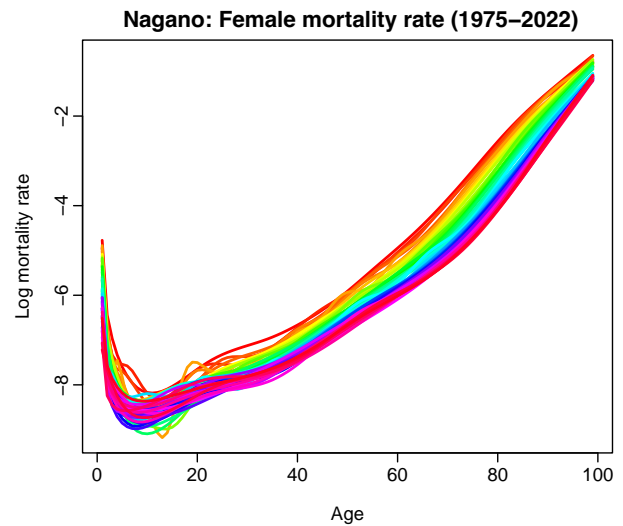
We evaluate and compare the forecasting accuracy of the proposed method with several competing methods. Further, we estimate life annuity pricing to demonstrate the impact of the forecasting improvement from the proposed method.

7.1 Japanese subnational age-specific mortality

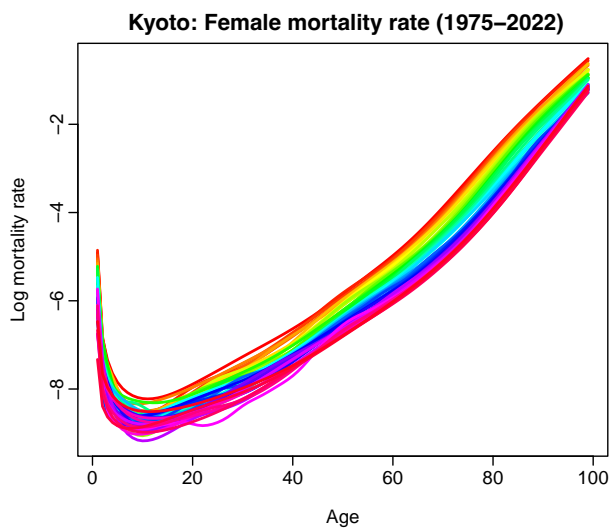
Figure 1 depicts the rainbow plots of the logarithm of the smoothed female mortality rates for four prefectures of Japan, namely, Tokyo, Nagano, Kyoto and Osaka, from 1975 to 2022. The rainbow plots of [Hyndman and Shang \(2010\)](#) can visualize a time ordering of functions. The colour order of the rainbow reflects the time ordering of the functional observations. Functions from the distant past are depicted in red, whereas more recent functions are shown in purple.



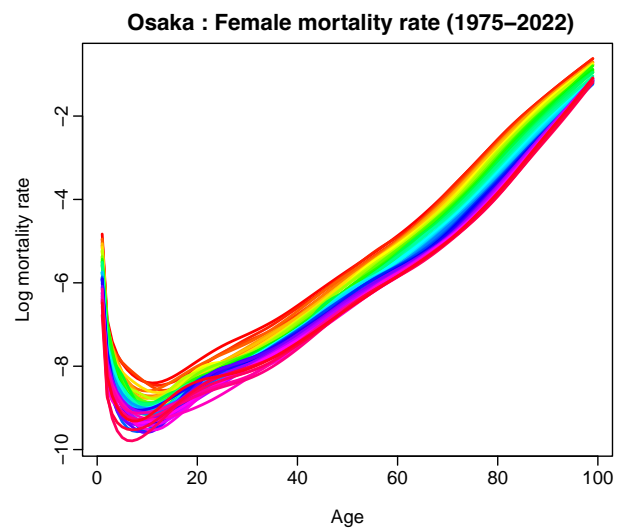
(a) Female smoothed mortality rates in Tokyo



(b) Female smoothed mortality rates in Nagano



(c) Female smoothed mortality rates in Kyoto



(d) Female smoothed mortality rates in Osaka

Figure 1: Functional time series displays for smoothed age-specific mortality rates of selected prefectures in Japan.

The weighted penalized regression splines method is applied to convert the observed data into continuous functions. Due to the sparsity of data for very high age group, we have aggregated both female and male mortality for ages over 98, hence the number of grid points on the mortality curves is 99.

Despite the general shapes of mortality rates for these four prefectures being similar, we may observe significant differences in the troughs and peaks and the overlaps of the curves. This indicates the mortality rates of different prefectures contain heterogeneity. To achieve improved forecasts of the subnational mortality rates, we need to extract the common features and use these common features to produce forecasts. This could be achieved by separating the homogeneity

and heterogeneity of mortality rates of all prefectures. From (3.4), the heterogeneity of mortality rates of each prefecture is reflected in $\Lambda(u)$, the $N \times k$ functional factor loading matrix, since each prefecture has a different set of functional factor loading. The term $\phi(u)F_t$ represents the homogeneity, which is common to all FTS.

Figure 2 shows the first four functional factor loadings of mortality rates of four chosen prefectures. All these four-factor loadings are different for these four prefectures. This represents the heterogeneity in the subnational mortality rates with different troughs, peaks and overlaps of the mortality rate curves.

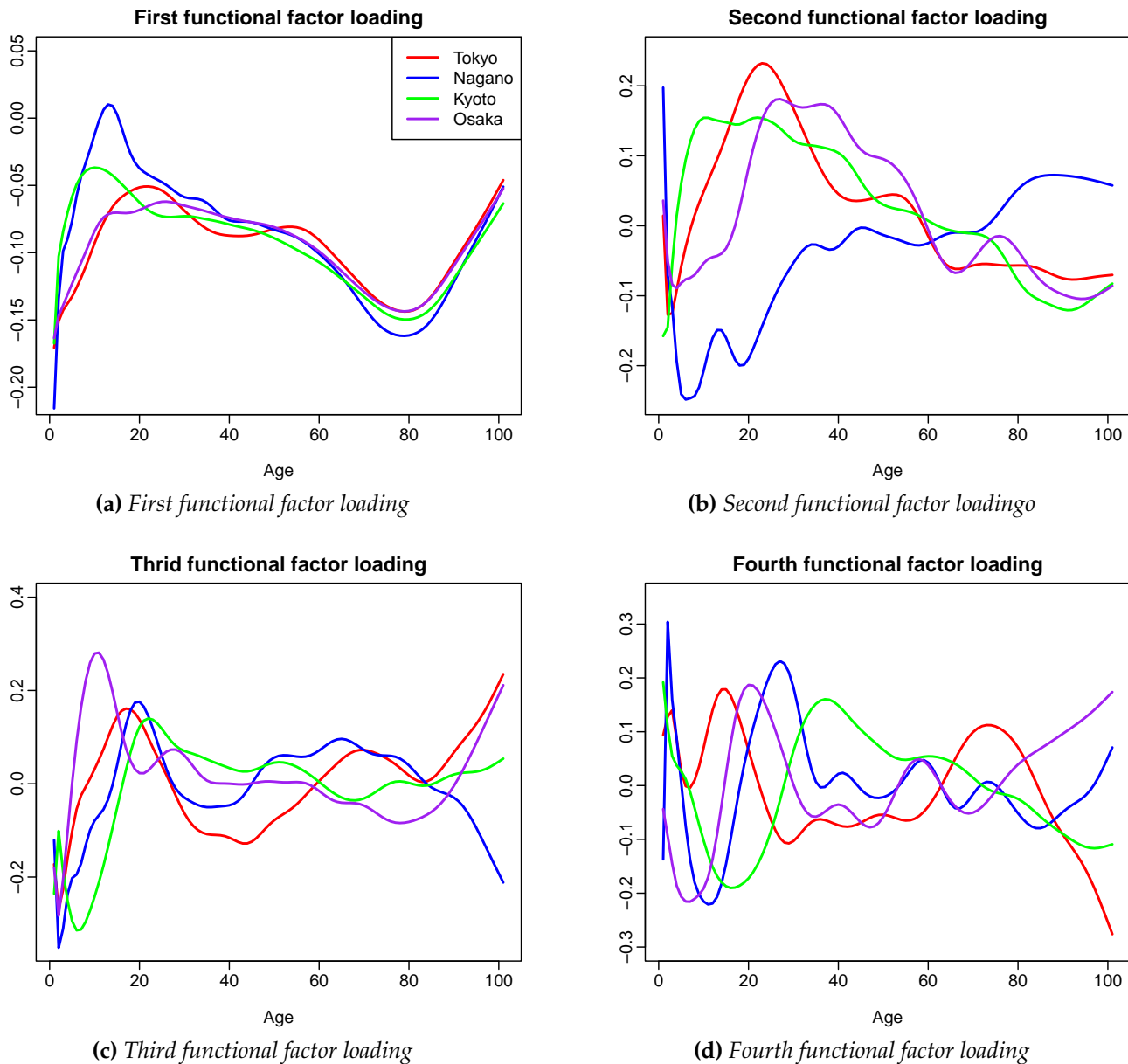


Figure 2: The first four functional factor loadings for four prefectures of Japan, namely Tokyo, Nagano, Kyoto and Osaka.

After separating the heterogeneity, we extract the common features in Figure 3, which are common to all mortality rate curves. This reflects the general common shapes and colour ordering of the mortality rates of all prefectures of Japan. By extracting the common features, we have reduced the dimension of the FTS of 47 prefectures of Japan into smaller sets of FTS. The temporal information within the original HDFTS is preserved in the fixed-dimensional FTS.

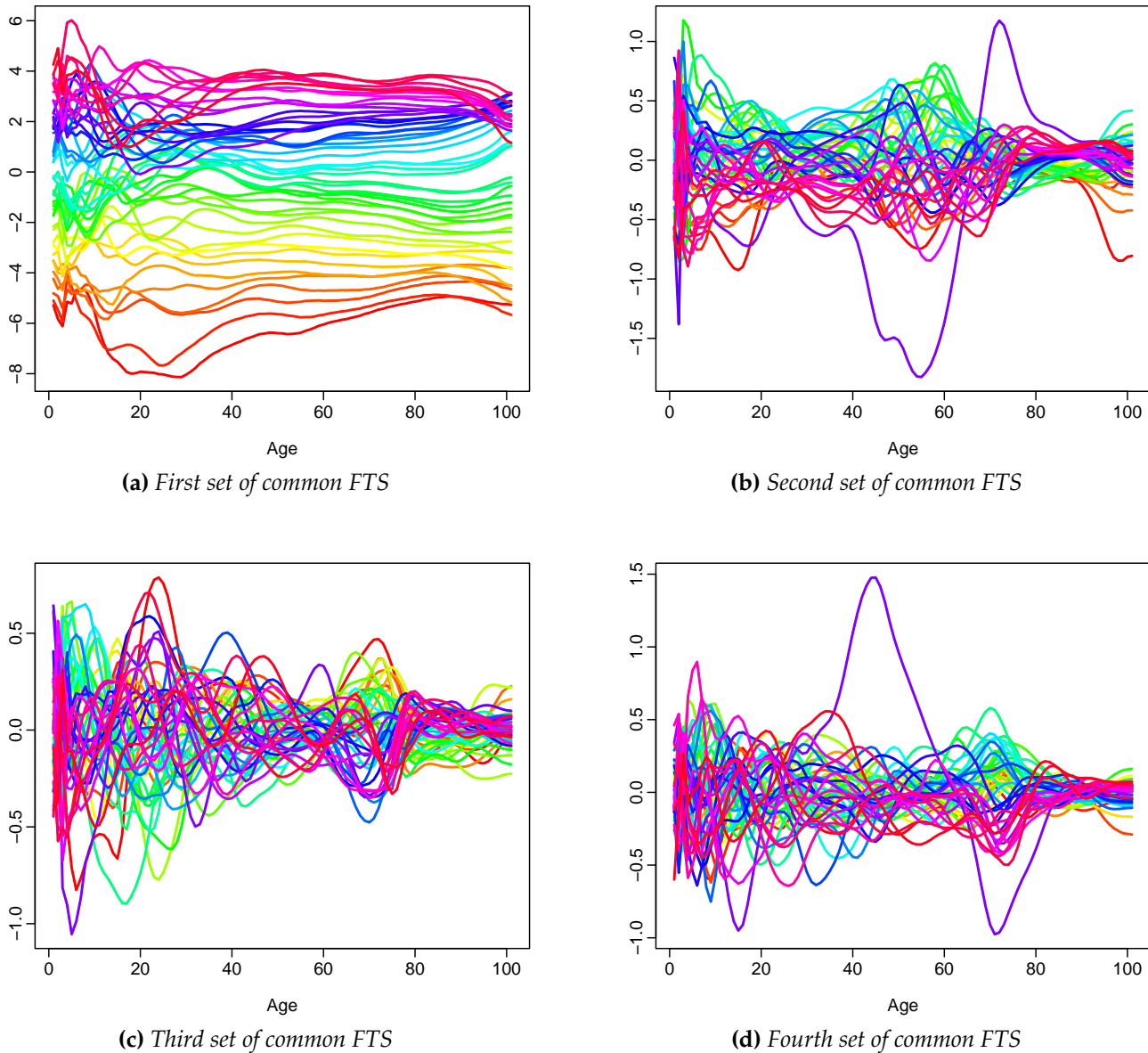


Figure 3: First four sets of common FTS of selected prefectures (Tokyo, Nagano, Kyoto and Osaka) in Japan.

In addition, the first four common functional factor loadings of both genders are depicted in Figure 4. Despite the general shape being similar for males and females, the common functional loadings for males contains more troughs and peaks, indicating that male mortality rates are more volatile than those of females.

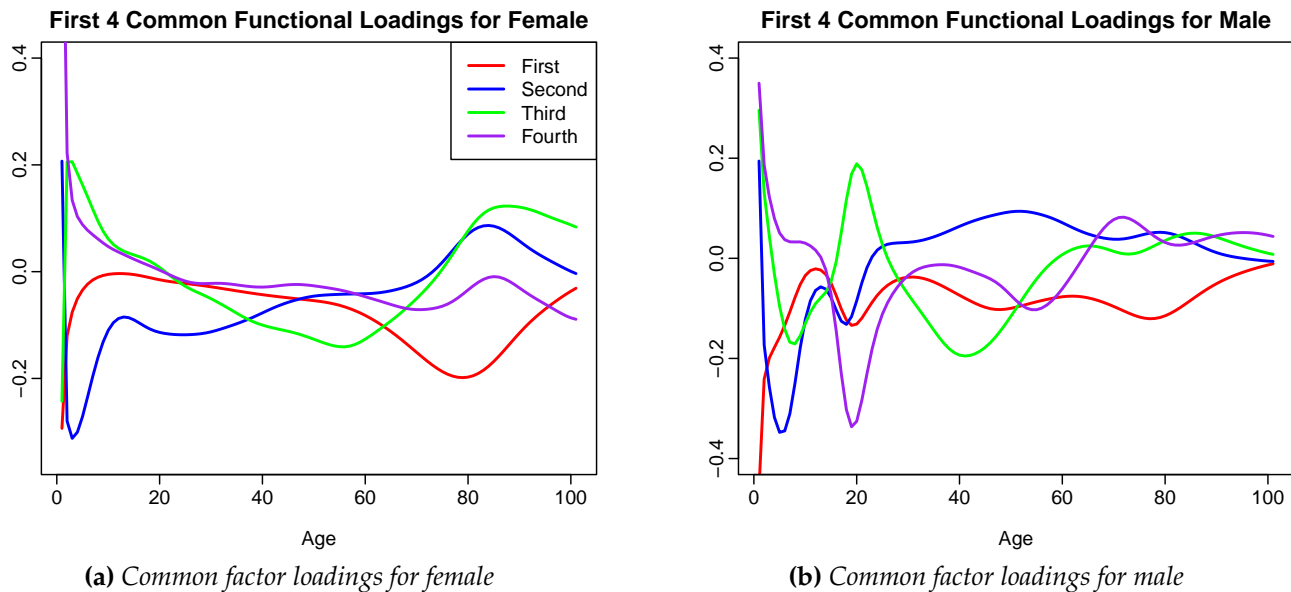


Figure 4: The first four common factor loadings for female and male data

Table 3 presents the first six eigenvalues for the auto-cross-covariance function of the common FTS and the long-run-covariance function of the FTS of four selected prefectures for both genders. The eigenvalues are normalized so that the sum of all eigenvalues adds up to one to reflect the percentage of total variation explained. We observe that the first few factors would explain most of the variations in the data.

Table 3: The first six normalized eigenvalues for the auto-cross-covariance function of the common FTS and the long-run-covariance function of four selected prefectures for both genders are reported. The eigenvalues for the auto-cross-covariance function of the common FTS are labelled as “Common”, and the eigenvalues for the long-run-covariance function of the FTS are labelled as “Specific”.

| Eigenvalue | Female | | | | | Male | | | | |
|-----------------|--------|----------|--------|-------|-------|--------|----------|--------|-------|-------|
| | Common | Specific | | | | Common | Specific | | | |
| | | Tokyo | Nagano | Kyoto | Osaka | | Tokyo | Nagano | Kyoto | Osaka |
| 1 st | 0.901 | 0.973 | 0.957 | 0.961 | 0.971 | 0.873 | 0.959 | 0.933 | 0.937 | 0.956 |
| 2 nd | 0.055 | 0.018 | 0.026 | 0.018 | 0.016 | 0.048 | 0.019 | 0.024 | 0.029 | 0.024 |
| 3 rd | 0.023 | 0.004 | 0.007 | 0.010 | 0.006 | 0.032 | 0.012 | 0.015 | 0.013 | 0.008 |
| 4 th | 0.008 | 0.002 | 0.004 | 0.005 | 0.004 | 0.021 | 0.004 | 0.009 | 0.008 | 0.005 |
| 5 th | 0.007 | 0.001 | 0.002 | 0.003 | 0.002 | 0.009 | 0.002 | 0.005 | 0.005 | 0.003 |
| 6 th | 0.003 | 0.001 | 0.001 | 0.002 | 0.001 | 0.006 | 0.001 | 0.005 | 0.003 | 0.002 |
| Sum | 0.997 | 0.999 | 0.997 | 0.999 | 1.000 | 0.989 | 0.997 | 0.991 | 0.995 | 0.998 |

The numbers of factors that we select for the common and specific FTS are four and six, respectively, for females and seven and eight, respectively, for males. With these selections of the number of factors, we ensure that the factors explain 99% of the variation in the data. Moreover, the percentages of total variation explained by the first factor for males are smaller than those for females, and this also explains that the data for males are more volatile.

7.2 Forecast evaluation

We consider the Japanese sub-national mortality data between 1975–2022 in the empirical study. To assess model and parameter stabilities over time, we adopt an expanding window analysis (see [Zivot and Wang, 2006](#), Chapter 9 for details) and produce forecasts in iterations. Specifically, we initiate the process by fitting the proposed HDFTS method to the first 38 years of observations between 1975–2012 and generating one- to 10-step-ahead point forecasts. Through an expanding window approach, we re-estimate the parameters of the considered model using the first 39 mortality curves from 1975 to 2013 and make one- to nine-step-ahead forecasts. The process is iterated with the sample size increased by one year until the end of the observation period. This process produces ten one-step-ahead forecasts, nine two-step-ahead forecasts, and so on, up to one 10-step-ahead forecast.

We compare the proposed method with the HDFTS studied in [Gao et al. \(2019\)](#), the high-dimensional functional factor model (HDFFM, [Tavakoli et al., 2023](#)), the two-step high-dimensional functional time series model (TSHDFTS [Chang et al., 2024](#)) the factor models for matrix-valued high-dimensional time series (MFM, [Wang et al., 2019](#)) and the tensor decomposition forecast methods (Canonical Polyadic Decomposition (CPD) and Tucker of [Dong et al. \(2020\)](#)).

7.2.1 Point forecast accuracy

We use the root mean square forecast error (RMSFE) to evaluate the point forecast accuracy. The RMSFE measures how close the forecast results are to the actual values of the data under forecast. The RMSFE for the h -step-ahead forecasts of the i^{th} prefecture for $i \in \{1, \dots, 47\}$ can be written as

$$\text{RMSFE}^{(i)}(h) = \sqrt{\frac{1}{J \times (T - n - h + 1)} \sum_{\kappa=n}^{T-h} \sum_{m=1}^{101} [\mathcal{X}_{\kappa+h}^{(i)}(u_m) - \hat{\mathcal{X}}_{\kappa+h|\kappa}^{(i)}(u_m)]^2},$$

where κ is the number of observations used in generating the point forecasts, $\mathcal{X}_{\kappa+h}^{(i)}(u_j)$ is the actual value of the $(\kappa + h)^{\text{th}}$ curve of the i^{th} prefecture, $\hat{\mathcal{X}}_{\kappa+h}^{(i)}(u_j)$ is the h -step-ahead point forecast based on the first κ observations, and J is the number of grid points on each curve. We use the average RMSFE for the h -step-ahead forecasts across all prefectures to reflect the accuracy of the h -step-ahead point forecasts:

$$\overline{\text{RMSFE}}(h) = \frac{1}{N} \sum_{i=1}^N \text{RMSFE}^{(i)}(h).$$

Table 4 tabulates the average RMSFE values across all prefectures for one-step ahead to 10-step ahead forecasts of different forecast methods. The bold entries highlight the method that produces the most accurate point forecast. Forecasts based on the proposed method have the smallest average RMSFE for both male and female mortality, which indicates that the proposed method outperforms other methods in terms of point forecast. This implies that the proposed model extracts the most information contained in the HDFTS.

Table 4: Average RMSE values ($\times 100$) in the holdout sample based on various forecasting methods are presented. Forecasts based on the proposed method are labelled as “FDFM”, forecasts based on high-dimensional functional time series are labelled as “HDFTS”, forecasts based on the two-step high-dimensional functional time series model are labelled as “TSHDFTS”, forecasts based on high-dimensional functional factor models are labelled as “HDFFM”, forecasts based on matrix factor models are labelled as “MFM”, forecasts based on CPD tensor decompositions are labelled as “CPD” and forecasts based on Tucker tensor decompositions are labelled as “Tucker”.

| Sex | h | FDFM | TSHDFTS | HDFTS | HDFFM | MFM | CPD | Tucker |
|--------|------|--------------|---------|-------|-------|-------|--------|--------------|
| Female | 1 | 0.641 | 0.723 | 2.165 | 2.272 | 1.464 | 0.755 | 0.741 |
| | 2 | 0.653 | 0.737 | 2.225 | 2.208 | 1.496 | 0.745 | 0.737 |
| | 3 | 0.655 | 0.755 | 2.268 | 2.261 | 1.518 | 0.730 | 0.703 |
| | 4 | 0.715 | 0.772 | 2.319 | 2.362 | 1.537 | 0.761 | 0.729 |
| | 5 | 0.691 | 0.801 | 2.360 | 2.397 | 1.553 | 0.770 | 0.774 |
| | 6 | 0.723 | 0.787 | 2.420 | 2.499 | 1.582 | 0.739 | 0.739 |
| | 7 | 0.815 | 0.797 | 2.470 | 2.513 | 1.601 | 0.741 | 0.740 |
| | 8 | 0.817 | 0.842 | 2.516 | 2.698 | 1.617 | 0.810 | 0.809 |
| | 9 | 0.666 | 0.924 | 2.413 | 2.921 | 1.488 | 0.840 | 0.833 |
| | 10 | 0.722 | 1.141 | 2.199 | 3.296 | 1.261 | 0.839 | 0.857 |
| | Mean | 0.710 | 0.828 | 2.336 | 2.543 | 1.512 | 0.773 | 0.776 |
| Male | 1 | 0.998 | 2.444 | 2.119 | 2.627 | 2.970 | 2.703 | 2.730 |
| | 2 | 1.004 | 2.516 | 2.172 | 2.725 | 2.866 | 2.7663 | 2.790 |
| | 3 | 1.030 | 2.536 | 2.218 | 2.772 | 2.836 | 2.783 | 2.821 |
| | 4 | 1.053 | 2.642 | 2.258 | 2.637 | 2.911 | 2.795 | 2.810 |
| | 5 | 1.086 | 2.850 | 2.304 | 2.508 | 2.794 | 2.812 | 2.842 |

| | | | | | | | |
|------|--------------|-------|-------|-------|-------|-------|-------|
| 6 | 1.093 | 3.006 | 2.372 | 2.422 | 2.917 | 2.841 | 2.869 |
| 7 | 1.112 | 3.161 | 2.432 | 2.484 | 3.149 | 2.865 | 2.905 |
| 8 | 1.138 | 2.634 | 2.473 | 2.496 | 2.937 | 2.913 | 2.954 |
| 9 | 1.290 | 1.601 | 2.322 | 2.358 | 2.798 | 2.892 | 2.952 |
| 10 | 1.578 | 2.119 | 2.025 | 2.052 | 2.968 | 2.682 | 2.756 |
| Mean | 1.138 | 2.551 | 2.270 | 2.508 | 2.915 | 2.805 | 2.843 |

7.2.2 Interval forecast accuracy

We use the interval scoring rule of [Gneiting and Raftery \(2007\)](#) and [Gneiting and Katzfuss \(2014\)](#) to evaluate point-wise interval forecast accuracy. The interval score for the point-wise prediction interval of the i^{th} prefecture at time point u_j is

$$\begin{aligned}
S_\alpha \left[\widehat{\mathcal{X}}_{\kappa+h|\kappa}^{(i),\text{lb}}(u_m), \widehat{\mathcal{X}}_{\kappa+h|\kappa}^{(i),\text{ub}}(u_m); \mathcal{X}_{\kappa+h}^{(i)}(u_m) \right] &= \left[\widehat{\mathcal{X}}_{\kappa+h|\kappa}^{(i),\text{ub}}(u_m) - \widehat{\mathcal{X}}_{\kappa+h|\kappa}^{(i),\text{lb}}(u_m) \right] \\
&+ \frac{2}{\alpha} \left[\widehat{\mathcal{X}}_{\kappa+h|\kappa}^{(i),\text{lb}}(u_m) - \mathcal{X}_{\kappa+h}^{(i)}(u_m) \right] \mathbb{1} \left\{ \mathcal{X}_{\kappa+h}^{(i)}(u_m) < \widehat{\mathcal{X}}_{\kappa+h|\kappa}^{(i),\text{lb}}(u_m) \right\} \\
&+ \frac{2}{\alpha} \left[\mathcal{X}_{\kappa+h}^{(i)}(u_m) - \widehat{\mathcal{X}}_{\kappa+h|\kappa}^{(i),\text{ub}}(u_m) \right] \mathbb{1} \left\{ \mathcal{X}_{\kappa+h}^{(i)}(u_m) > \widehat{\mathcal{X}}_{\kappa+h|\kappa}^{(i),\text{ub}}(u_m) \right\},
\end{aligned}$$

where the level of significance α can be chosen conventionally as 0.2. It is not difficult to find that the smaller the interval score, the more accurate the interval forecast. An optimal (which is also minimal) interval score value can be achieved if $\mathcal{X}_{\kappa+h}^{(i)}(u_j)$ lies between $\widehat{\mathcal{X}}_{\kappa+h|\kappa}^{(i),\text{lb}}(u_j)$ and $\widehat{\mathcal{X}}_{\kappa+h|\kappa}^{(i),\text{ub}}(u_j)$. Then the mean interval score for the h -step-ahead forecasts of the i^{th} prefecture can be written as

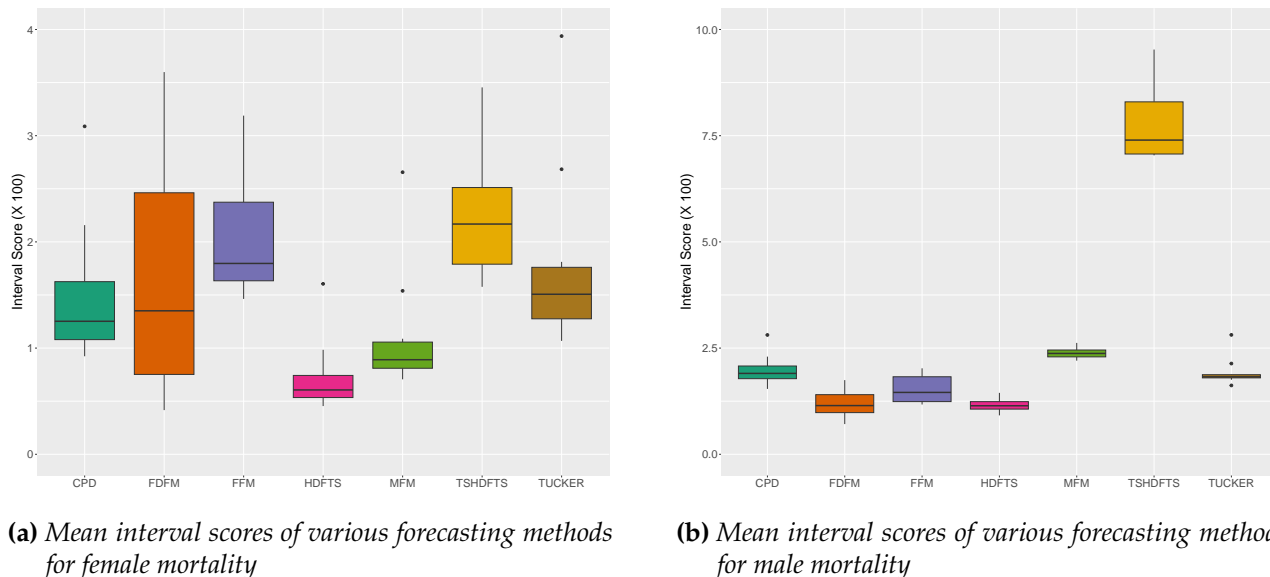
$$\bar{S}_\alpha^{(i)}(h) = \frac{1}{101 \times (T - n - h + 1)} \sum_{\kappa=n}^{T-h} \sum_{m=1}^{101} S_\alpha \left[\widehat{\mathcal{X}}_{\kappa+h|\kappa}^{(i),\text{lb}}(u_m), \widehat{\mathcal{X}}_{\kappa+h|\kappa}^{(i),\text{ub}}(u_m); \mathcal{X}_{\kappa+h}^{(i)}(u_m) \right].$$

We use the average mean interval score for the h -step-ahead forecasts across all prefectures to reflect the accuracy of the h -step-ahead point-wise prediction interval:

$$\bar{S}_\alpha(h) = \frac{1}{N} \sum_{i=1}^N \bar{S}_\alpha^{(i)}(h).$$

Figure 5 shows the side-by-side box plots of average mean interval score values across all prefectures for one-step ahead to 10-step ahead forecasts of different forecast methods. From the box plots, despite HDFTS performing better for female mortality, the proposed method performs relatively the same as HDFTS, which indicates the proposed method could generate relatively smaller average mean interval score values for some of the forecast horizons. This demonstrates

that the proposed method is capable of producing more accurate interval forecasts.



(a) Mean interval scores of various forecasting methods for female mortality

(b) Mean interval scores of various forecasting methods for male mortality

Figure 5: Average interval score values ($\times 100$) in the holdout sample of various forecasting methods

After comparing the point and interval forecast results of various methods, we found that our proposed method outperforms other competitive methods in forecasting the HDFTS. This indicates that the proposed model’s dimension reduction process efficiently captures both the serial dependence and the correlation among cross sections in the HDFTS.

7.2.3 Computation Speed

We also compare the computational speed of various high-dimensional mortality forecasting methods. The methods shown in Table 5 are applied to the same training dataset sequentially to obtain one-step-ahead point forecasts, with their computation time in seconds recorded. It is worth noting that CPD’s fast computation speed is due to the time efficiency of Tucker’s decomposition embedded in the algorithm. Our proposed method takes 50% – 90% more time to implement compared to other functional data analysis approaches shown in the table. However, the superior forecasting accuracy of the proposed FDFM method justifies the additional computation time. The TSHDFTS method of Chang et al. (2024) selects parameters by cross-validations, which requires significant computation time in implementation. For this reason, we left the method out of the comparison presented in the table.

Table 5: Computational time (in seconds) of the considered high-dimensional mortality forecasting methods.

| | Model | Computation Time (seconds) |
|------------------------|--------|----------------------------|
| Our method | FDFM | 187.12 |
| Gao et al. (2019) | HDFTS | 68.95 |
| Wang et al. (2019) | MFM | 95.94 |
| Dong et al. (2020) | CPD | 0.20 |
| Dong et al. (2020) | Tucker | 0.39 |
| Tavakoli et al. (2023) | HDFFM | 108.14 |

7.3 Life annuity Pricing

Life annuities are one of the typical longevity insurance products for retirees, helping them finance their retirements. Rapid improvements in mortality have exposed life insurers to longevity risk (Ngai and Sherris, 2011). Accurate mortality forecasts could enable life insurers to manage longevity risk effectively without holding excessive levels of capital. To illustrate the impact of these forecasting improvements, we use the mortality forecasts to price life annuities, that is, the amount of money an individual pays to a life insurer in return for annual payments after retirement until death. We compare the present values of the life annuities, that is, the amount of capital the life insurer should reserve, based on mortality forecasts from different methods.

In comparing the value of a life annuity, we calculate the present value (PV) of the life annuity with \$1 annual payments. More specifically, the price of a life annuity for an individual aged x at year t is the PV of the annual payments of \$1 that the individual receives after retirement until death or a pre-agreed age (whichever occurs first). The retirement age is set to be 65, and the pre-agreed age at which the annuity terminates is assumed to be 90 (He et al., 2021). Then the price of the annuity can be calculated as follows:

$$PV_{x,t} = \begin{cases} \sum_{n=1}^{90-x} \frac{{}_n p_{x,t}}{(1+i)^n}, & x \geq 65 \\ \sum_{n=1}^{25} \frac{{}_n p_{65,t+(65-x)}}{(1+i)^{n+(65-x)}}, & x < 65, \end{cases}$$

where $PV_{x,t}$ is the PV of the life annuity for an individual aged x at year t , ${}_n p_{x,t}$ is the survival probability for an individual aged x at year t to survive after n years, and i is the interest rate used

for discounting. An individual older than 65-year-old receives payment for each year of survival, and for an individual younger than 65-year-old, the annuity is deferred with the first payment paid out at the year that they survive their 66th birthday.

To demonstrate the financial impact of the forecasting improvement in mortality, we compare annuity prices based on mortality forecasting using different methods. We use the Japanese sub-national mortality data of 47 prefectures from 1975 to 2012 as the training dataset and the data from the years 2013 to 2022 as testing data. We forecast the mortality rates for the testing data based on the training data using different methods. Then we calculate the annuity prices, $PV_{x,t}$ using the forecasts of mortality rates from different methods as well as the actual mortality rates.

Table 6 exhibits the average prices of annuities with annual payment \$1 and interest rate 2% in Japan for some selected ages and years. Most forecasting methods tend to underestimate annuity prices, which is a common phenomenon in actuarial science, corresponding to the underestimated longevity risk (Ngai and Sherris, 2011). Comparably, our methods slightly overestimate annuity prices. Further investigation of annuity prices reveals that the pricing errors of the proposed method are much lower than those of other methods.

Table 6: Average annuity prices with annual payment \$1 and interest rate 2% in Japan for selected ages and years. Annuity prices based on true mortality rates are labelled as "TRUE", annuity prices based on the proposed method are labelled as "FDFM", annuity prices based on high-dimensional functional time series are labelled as "HDFTS", annuity prices based on high-dimensional functional factor models are labelled as "HDFFM", annuity prices based on a matrix factor model are labelled as "MFM", annuity prices based on CPD tensor decompositions are labelled as "CPD" and annuity prices based on Tucker tensor decompositions are labelled as "Tucker".

| Sex | (Year, Age) | TRUE | FDFM | HDFTS | HDFFM | MFM | CPD | Tucker |
|--------|-------------|--------|--------|--------|--------|--------|--------|--------|
| Female | (1980, 55) | 13.026 | 13.032 | 12.964 | 12.940 | 12.997 | 13.040 | 13.035 |
| | (1985, 60) | 14.724 | 14.731 | 14.654 | 14.627 | 14.691 | 14.740 | 14.734 |
| | (1990, 65) | 15.786 | 15.794 | 15.707 | 15.676 | 15.749 | 15.805 | 15.798 |
| | (1995, 70) | 12.980 | 12.989 | 12.888 | 12.852 | 12.937 | 13.001 | 12.994 |
| | (2000, 75) | 10.042 | 10.053 | 9.933 | 9.890 | 9.990 | 10.067 | 10.058 |
| | (2005, 80) | 6.976 | 6.990 | 6.840 | 6.787 | 6.912 | 7.007 | 6.996 |
| | (2010, 85) | 3.776 | 3.795 | 3.590 | 3.518 | 3.688 | 3.819 | 3.804 |
| Male | (1980, 55) | 10.081 | 10.085 | 10.057 | 10.057 | 10.067 | 10.090 | 10.090 |
| | (1985, 60) | 11.698 | 11.702 | 11.670 | 11.670 | 11.682 | 11.708 | 11.708 |
| | (1990, 65) | 12.863 | 12.869 | 12.830 | 12.830 | 12.844 | 12.876 | 12.875 |
| | (1995, 70) | 10.411 | 10.418 | 10.371 | 10.370 | 10.388 | 10.427 | 10.426 |
| | (2000, 75) | 7.981 | 7.990 | 7.928 | 7.928 | 7.950 | 8.001 | 8.001 |
| | (2005, 80) | 5.571 | 5.584 | 5.495 | 5.495 | 5.527 | 5.600 | 5.599 |
| | (2010, 85) | 3.161 | 3.182 | 3.031 | 3.029 | 3.085 | 3.210 | 3.209 |

To illustrate the financial impact of the mispricing on life insurers, consider the annuity pricing for females aged 75 at year 2000. The pricing error for the proposed method is \$0.011 per \$1 payment. However, the pricing errors for other competing methods range from \$0.016 to \$0.152 per \$1 payment. Suppose the annual payment for each individual is \$10,000, and 50,000 people purchased this product. Then based on the proposed method, the capital that the insurer needs to reserve is reduced by at least 26 million $\left((\$0.016 - \$0.011) \times 10,000 \times 50,000 = \$2.5\text{million} \right)$, a significant saving to the life insurer.

8 Conclusion

We propose a factor model for HDFTS. By identifying homogeneity, we can reduce the HDFTS into an FTS of low dimensions. Then, a common functional front-loading can be determined to extract the temporal information in HDFTS into a low-dimensional FTS. The proposed model provides more flexibility, with certain choices of front and back-loadings; our model coincides with some of the existing factor models for HDFTS.

Via a series of Monte-Carlo simulations, we demonstrate the performance of the proposed method for in-sample model fitting and out-of-sample forecast accuracy. An empirical study on the age-specific mortality rates of 47 Japanese prefectures demonstrates the superiority of the proposed method over the existing models in forecasting. This result shows that the proposed model can extract temporal information more effectively.

The proposed model can be viewed as a functional panel data model with interactive effects. We considered the multiplicity of time trend effects and population-specific effects instead of addition as in additive fixed effects models.

In the current work, functional concurrent regression is performed for each $t \in \{1, \dots, T\}$ to obtain the FTS of lower dimensions, which omits the temporal dependence of the functional observations. A possible future study could extend our functional concurrent regression to the FTS regression of [Pham and Panaretos \(2018\)](#). This awaits further investigation.

Acknowledgment

This research was financially supported by the Australian Research Council Discovery Project (DP230102250). The usual disclaimer applies.

References

- Andrews, D. (1991), 'Heteroskedasticity and autocorrelation consistent covariant matrix estimation', *Econometrica* **59**(3), 817–858.
- Bai, J. (2009), 'Panel data models with interactive fixed effects', *Econometrica* **77**(4), 1229–1279.
- Bai, J. and Ng, S. (2008), 'Large dimensional factor analysis', *Foundations and Trends® in Econometrics* **3**(2), 89–163.
- Bathia, N., Yao, Q., Ziegelmann, F. et al. (2010), 'Identifying the finite dimensionality of curve time series', *The Annals of Statistics* **38**(6), 3352–3386.
- Bellman, R. (1966), 'Dynamic programming', *Science* **153**(3731), 34–37.
- Bühlmann, P. and van de Geer, S. (2011), *Statistics for High-dimensional Data: Methods, Theory and Applications*, Springer Science & Business Media, Berlin.
- Cai, T. and Chen, X. (2010), *High-dimensional Data Analysis*, Higher Education Press, Beijing.
- Chang, J., Fang, Q., Qiao, X. and Yao, Q. (2024), On the modelling and prediction of high-dimensional functional time series, LSE Working Paper, arXiv.
URL: <https://personal.lse.ac.uk/qiaox/qiao.links/PredictHFTS.pdf>
- Chiou, J.-M. (2012), 'Dynamical functional prediction and classification, with application to traffic flow prediction', *The Annals of Applied Statistics* **6**(4), 1588–1614.
- Di, C.-Z., Crainiceanu, C. M., Caffo, B. S. and Punjabi, N. M. (2009), 'Multilevel functional principal component analysis', *The Annals of Applied Statistics* **3**(1), 458–488.
- Dong, Y., Huang, F., Yu, H. and Haberman, S. (2020), 'Multi-population mortality forecasting using tensor decomposition', *Scandinavian Actuarial Journal* **2020**, 754–775.

- Freyberger, J. (2018), 'Non-parametric panel data models with interactive fixed effects', *The Review of Economic Studies* **85**(3), 1824–1851.
- Gallant, A. R. (2009), *Nonlinear Statistical Models*, John Wiley & Sons, Hoboken, New Jersey.
- Gao, Y., Shang, H. L. and Yang, Y. (2019), 'High-dimensional functional time series forecasting: An application to age-specific mortality rates', *Journal of Multivariate Analysis* **170**, 232–243.
- Gneiting, T. and Katzfuss, M. (2014), 'Probabilistic forecasting', *Annual Review of Statistics and Its Application* **1**, 125–151.
- Gneiting, T. and Raftery, A. E. (2007), 'Strictly proper scoring rules, prediction, and estimation', *Journal of the American Statistical Association: Review Article* **102**(477), 359–378.
- Hall, P. and Vial, C. (2006), 'Assessing the finite dimensionality of functional data', *Journal of the Royal Statistical Society: Series B (Statistical Methodology)* **68**(4), 689–705.
- Hansen, L. P. (1982), 'Large sample properties of generalized method of moments estimators', *Econometrica* **50**(4), 1029–1054.
- He, L., Huang, F. and Yang, Y. (2021), Data-adaptive dimension reduction for US mortality forecasting, Technical report, arXiv preprint.
URL: <https://arxiv.org/abs/2102.04123>
- Hörmann, S. and Kidziński, Ł. (2015), 'A note on estimation in Hilbertian linear models', *Scandinavian Journal of Statistics* **42**(1), 43–62.
- Hörmann, S., Kidziński, Ł. and Hallin, M. (2015), 'Dynamic functional principal components', *Journal of the Royal Statistical Society: Series B (Statistical Methodology)* **77**(2), 319–348.
- Hörmann, S. and Kokoszka, P. (2010), 'Weakly dependent functional data', *The Annals of Statistics* **38**(3), 1845–1884.
- Horváth, L. and Kokoszka, P. (2012), *Inference For Functional Data with Applications*, Springer Science & Business Media, New York.
- Horváth, L., Kokoszka, P. and Reeder, R. (2013), 'Estimation of the mean of functional time series and a two-sample problem', *Journal of the Royal Statistical Society: Series B (Statistical Methodology)* **75**(1), 103–122.

- Hyndman, R. J. and Shang, H. L. (2010), 'Rainbow plots, bagplots, and boxplots for functional data', *Journal of Computational and Graphical Statistics* **19**(1), 29–45.
- Hyndman, R. J. and Ullah, M. S. (2007), 'Robust forecasting of mortality and fertility rates: A functional data approach', *Computational Statistics & Data Analysis* **51**(10), 4942–4956.
- Japan Mortality Database (2024), *National Institute of Population and Social Security Research*. Accessed at April 12, 2023.
URL: <http://www.ipss.go.jp/p-toukei/JMD/>
- Jiménez-Varón, C. F., Sun, Y. and Shang, H. L. (2024), 'Forecasting high-dimensional functional time series: Application to sub-national age-specific mortality', *Journal of Computational and Graphical Statistics* **in press**.
- Lam, C. and Yao, Q. (2012), 'Factor modeling for high-dimensional time series: Inference for the number of factors', *The Annals of Statistics* **40**(2), 694–726.
- Lam, C., Yao, Q. and Bathia, N. (2011), 'Estimation of latent factors for high-dimensional time series', *Biometrika* **98**(4), 901–918.
- Lee, R. D. and Carter, L. R. (1992), 'Modeling and forecasting U.S. mortality', *Journal of the American Statistical Association: Application & Case Studies* **87**(419), 659–671.
- Li, J. (2013), 'A Poisson common factor model for projecting mortality and life expectancy jointly for females and males', *Population Studies* **67**(1), 111–126.
- Li, N. and Lee, R. (2005), 'Coherent mortality forecasts for a group of populations: An extension of the Lee-Carter method', *Demography* **42**(3), 575–594.
- Li, N., Lee, R. and Gerland, P. (2013), 'Extending the Lee-Carter method to model the rotation of age patterns of mortality decline for long-term projections', *Demography* **50**(6), 2037–2051.
- Newey, W. K. and West, K. D. (1987), 'A simple, positive semi-definite, heteroskedasticity and autocorrelation consistent covariance matrix', *Econometrica* **55**(3), 703–708.
- Ngai, A. and Sherris, M. (2011), 'Longevity risk management for life and variable annuities: the effectiveness of static hedging using longevity bonds and derivatives', *Insurance: Mathematics and Economics* **49**(1), 100–114.

- Pampel, F. (2005), 'Forecasting sex differences in mortality in high income nations: the contribution of smoking', *Demographic Research* **13**(18), 455–484.
- Panaretos, V. M. and Tavakoli, S. (2013), 'Fourier analysis of stationary time series in function space', *The Annals of Statistics* **41**(2), 568–603.
- Pham, T. and Panaretos, V. M. (2018), 'Methodology and convergence rates for functional time series regression', *Statistica Sinica* **28**(4), 2521–2539.
- Politis, D. N. and Romano, J. P. (1996), 'On flat-top kernel spectral density estimators for homogeneous random fields', *Journal of Statistical Planning and Inference* **51**(1), 41–53.
- Politis, D. N. and Romano, J. P. (1999), 'Multivariate density estimation with general flat-top kernels of infinite order', *Journal of Multivariate Analysis* **68**(1), 1–25.
- Ramsay, J. O., Hooker, G. and Graves, S. (2009), *Functional Data Analysis with R and MATLAB*, Springer, New York.
- Ramsay, J. O. and Silverman, B. W. (2006), *Functional Data Analysis*, Springer Science & Business Media, New York.
- Renshaw, A. E. and Haberman, S. (2003), 'Lee-Carter mortality forecasting with age-specific enhancement', *Insurance: Mathematics and Economics* **33**(2), 255–272.
- Rice, G. and Shang, H. L. (2017), 'A plug-in bandwidth selection procedure for long-run covariance estimation with stationary functional time series', *Journal of Time Series Analysis* **38**(4), 591–609.
- Rice, J. A. and Silverman, B. W. (1991), 'Estimating the mean and covariance structure nonparametrically when the data are curves', *Journal of the Royal Statistical Society. Series B (Statistical Methodology)* **53**(1), 233–243.
- Shang, H. L. (2016), 'Mortality and life expectancy forecasting for a group of populations in developed countries: A multilevel functional data method', *The Annals of Applied Statistics* **10**(3), 1639–1672.
- Shang, H. L. (2018), 'Bootstrap methods for stationary functional time series', *Statistics and Computing* **28**(1), 1–10.

- Tang, C., Shang, H. L. and Yang, Y. (2022), 'Clustering and forecasting multiple functional time series', *The Annals of Applied Statistics* **16**(4), 2523–2553.
- Tavakoli, S., Nisol, G. and Hallin, M. (2023), 'Factor models for high-dimensional functional time series II: Estimation and forecasting', *Journal of Time Series Analysis* **44**(5-6), 601–621.
- Tsay, R. S. (2013), *Multivariate Time Series Analysis: with R and Financial Applications*, John Wiley & Sons, New York.
- Wang, D., Liu, X. and Chen, R. (2019), 'Factor models for matrix-valued high-dimensional time series', *Journal of Econometrics* **208**(1), 231–248.
- White, H. (1984), *Asymptotic Theory for Econometricians*, Academic press, Cambridge, Massachusetts.
- Wiśniowski, A., Smith, P. W., Bijak, J., Raymer, J. and Forster, J. J. (2015), 'Bayesian population forecasting: Extending the Lee-Carter method', *Demography* **52**(3), 1035–1059.
- Yang, Y., Shang, H. L., Cohen, J. E. et al. (2022), 'Temporal and spatial Taylor's law: Application to Japanese subnational mortality rates', *Journal of the Royal Statistical Society Series A* **185**(4), 1979–2006.
- Yao, F., Müller, H.-G. and Wang, J.-L. (2005), 'Functional data analysis for sparse longitudinal data', *Journal of the American Statistical Association: Theory and Methods* **100**(470), 577–590.
- Zhou, Z. and Dette, H. (2023), 'Statistical inference for high-dimensional panel functional time series', *Journal of the Royal Statistical Society Series B: Statistical Methodology* **85**(2), 523–549.
- Zivot, E. and Wang, J. (2006), *Modeling financial time series with S-PLUS*, Vol. 2, Springer, New York.